RESEARCH ARTICLE

GFAP expression in the optic nerve and increased H_2S generation in the integration centers of the rainbow trout (*Oncorhynchus mykiss*) brain after unilateral eye injury

Evgeniya V. Pushchina[1, 2, *], Anatoly A. Varaksin[1], Dmitry K. Obukhov[3], Igor M. Prudnikov[2]

1 A.V. Zhirmunsky National Scientific Center of Marine Biology, Far Eastern Branch, Russian Academy of Sciences, Vladivostok, Russia

2 A.A. Bogomoletz Institute of Physiology, National Academy of Sciences of Ukraine, Kiev, Ukraine

3 St. Petersburg State University, St. Petersburg, Russia

Funding: *This work was supported by a grant from the President of the Russian Federation (No. MD-4318.2015.4; to EVP), a grant from the Program for Basic Research of the Far East Branch of the Russian Academy of Sciences 2015–2017 (No. 15-I-6-116, section III to EVP, AAV and DKO).*

Abstract

Hydrogen sulfide (H_2S) is considered as a protective factor against cardiovascular disorders. However, there are few reports on the effects of H_2S in the central nervous system during stress or injury. Previous studies on goldfish have shown that astrocytic response occurs in the damaged and contralateral optic nerves. Glial fibrillary acidic protein (GFAP) concentration in the optic nerves of rainbow trout has not been measured previously. This study further characterized the astrocytic response in the optic nerve and the brain of a rainbow trout (*Oncorhynchus mykiss*) after unilateral eye injury and estimated the amount of H_2S-producing enzyme cystathionine β-synthase (CBS) in the brain of the rainbow trout. Within 1 week after unilateral eye injury, a protein band corresponding to a molecular weight of 50 kDa was identified in the ipsi- and contralateral optic nerves of the rainbow trout. The concentration of GFAP in the injured optic nerve increased compared to the protein concentration on the contralateral side. The results of a quantitative analysis of $GFAP^+$ cell distribution in the contralateral optic nerve showed the largest number of $GFAP^+$ cells and fibers in the optic nerve head. In the damaged optic nerve, patterns of $GFAP^+$ cell migration and large $GFAP^+$ bipolar activated astrocytes were detected at 1 week after unilateral eye injury. The study of H_2S-producing system after unilateral eye injury in the rainbow trout was conducted using enzyme-linked immunosorbent assay, western blot analysis, and immunohistochemistry of polyclonal antibodies again st CBS in the integrative centers of the brain: telencephalon, optic tectum, and cerebellum. Enzyme-linked immunosorbent assay results showed a 1.7-fold increase in CBS expression in the rainbow trout brain at 1 week after unilateral eye injury compared with that in intact animals. In the ventricular and subventricular regions of the rainbow trout telencephalon, CBS^+ radial glia and neuroepithelial cells were identified. After unilateral eye injury, the number of CBS^+ neuroepithelial cells in the pallial and subpallial periventricular regions of the telencephalon increased. In the optic tectum, unilateral eye injury led to an increase in CBS expression in radial glial cells; simultaneously, the number of CBS^+ neuroepithelial cells decreased in intact animals. In the cerebellum of the rainbow trout, neuroglial interrelationships were revealed, where H_2S was released, apparently, from astrocyte-like cells. The organization of H_2S-producing cell complexes suggests that, the amount of glutamate produced in the rainbow trout cerebellum and its reuptake was controlled by astrocyte-like cells, reducing its excitotoxicity. In the dorsal matrix zone and granular eminences of the rainbow trout cerebellum, CBS was expressed in neuroepithelial cells. After unilateral eye injury, the level of CBS activity increased in all parts of the cerebellum. An increase in the number of H_2S-producing cells was a response to oxidative stress after unilateral eye injury, and the overproduction of H_2S in the cerebellum occurred to neutralize reactive oxygen species, providing the cells of the rainbow trout cerebellum with a protective effect. A structural reorganization in the dorsal matrix zone, associated with the appearance of an additional CBS^+ apical zone, and a decrease in the enzyme activity in the dorsal matrix zone, was revealed in the zones of constitutive neurogenesis. All experiments were approved by the Commission on Biomedical Ethics, A.V. Zhirmunsky National Scientific Center of Marine Biology (NSCMB), Far Eastern Branch, Russian Academy of Science (FEB RAS) (approval No. 1) on July 31, 2019.

Key Words: *astrocyte-like cells; glial fibrillary acidic protein; hydrogen sulfide; neuroepithelial cells; neuroprotection; radial glial cells; rainbow trout (Oncorhynchus mykiss); reactive oxygen species; unilateral eye injury*

Chinese Library Classification No. *R446; R364; R741*

Correspondence to:
Evgeniya V. Pushchina, DSci., PhD, puschina@mail.ru.

orcid:
0000-0003-0388-3147 (Evgeniya V. Pushchina)

doi: *10.4103/1673-5374.280320*

Received: *August 6, 2019*
Peer review started: *August 10, 2019*
Accepted: *December 12, 2019*
Published online: *April 3, 2020*

Introduction

Hydrogen sulfide (H_2S) has been identified as a gasotransmitter having antioxidant properties (Wang, 2012; Wang et al., 2014). To date, the vasodilatory, neuromodulatory, and anti-inflammatory actions of H_2S have been investigated (Kimura et al., 2012; Kimura, 2013; Liu et al., 2016). In studies of the cardiovascular system, H_2S functions were assumed to be a protective factor (Mergenthaler et al., 2004); however, in the central nervous system (CNS), the effects of H_2S during stress or injury remain poorly understood. The involvement of H_2S, as well as other gaseous intermediaries such as NO, CO, H_2, in traumatic brain injury is now intensively investigated (Olson et al., 2012; Deng et al., 2014), but to date this issue has not been completely clarified. H_2S, similarly to nitric oxide (NO), is known to mediate post-translational modification of proteins by adding extra sulfur atoms to reactive cysteine residues. This modification, referred to as S-sulfhydration, is required to activate or inactivate many classes of proteins, including ion channels such as ATP-dependent potassium channels, TRPV3, TRPV6, TRPM (Liu et al., 2014), enzymes and transcription factors NF-kB, Nrf2 (Paul and Snyder, 2012).

Progress in studies of H_2S biology has led to a conclusion that polysulfides are prevailing sources of intermediate sulfhydration of proteins than H_2S (Kimura et al., 2013). H_2S reactions with many signal mediators, transcription factors, and channel proteins in neurons and glial cells are known both *in vivo* and *in vitro* (Che et al., 2018; Gopalakrishnan et al., 2019). However, little is known about the participation of H_2S intercellular communication and its consequences in the case of a traumatic cerebral injury. Such information is necessary to identify the cytoprotective or cytotoxic effects of H_2S in brain injury and/or cerebral ischemia.

Recently, the involvement of H_2S in cerebral ischemia, traumatic brain injury (TBI), and the decreasing reactive oxygen species in H_2S-dependent mechanisms were studied in different models (Kalogeris et al., 2012; Che et al., 2018; Gopalakrishnan et al., 2019). The use of monoclonal antibodies against cystathionine β-synthase (CBS) for immunohistochemical detection of H2S-producing complexes in the brain of juvenile rainbow trout showed an increase in H_2S production in different parts of the brain and an induction of CBS in radial glia (RG) cells after injury of the optic nerve (Pushchina et al., 2019). The toxic and/or neuroprotective effects of H_2S depend on its concentration: lower concentrations of H_2S play a physiological role, while very high concentrations of H_2S cause cell death (Li et al., 2011; Jiang et al., 2013). Modulation of ion channels, inflammatory and antioxidant transcription factors with the involvement of H_2S after a traumatic brain injury can play a significant role in reducing edema and inflammation (Gopalakrishnan et al., 2019).

The study of the biology of neural stem cells in animal models is becoming increasingly important, since the processes of constitutive neurogenesis continue in many regions of the animal brain (Adolf et al., 2006; Ito et al., 2010; Than-Trong and Bally-Cuif, 2015), providing a high reparative potential of CNS. Fish are regenerative-competent organisms characterized by a high rate of reparative processes (Zupanc and Sirbulesku, 2011). In our previous study, we investigated the features of apoptosis in the optic nerve and the proliferative response in the cerebellum and in the optic tectum of rainbow trout with unilateral eye injury (UEI; Pushchina et al., 2016a). The results of preliminary studies showed an increase in proliferative activity of brain cells after UEI, which was also recorded during *in vitro* experiments (Pushchina et al., 2016b).

According to previous studies on a goldfish, the astrocytic response occurs in the damaged and contralateral optic nerves (Parilla et al., 2009). The results of immunoblotting of rainbow trout brain homogenates have shown the presence of two GFAP isoforms in the brain: light, with a molecular weight of 50–52 kDa, and heavy, 90 kDa (Alunni et al., 2005). The light isoform was found in rainbow trout larvae, as well as in the medulla and spinal cord of adult rainbow trout. The heavy isoform was identified predominantly in the adult rainbow trout forebrain, but was also characteristic of the whole larval brain homogenates (Alunni et al., 2005). GFAP concentration in the optic nerves of rainbow trout has not been measured previously.

To further characterize the astrocytic response in the optic nerve and the brain of a trout after UEI, variations in GFAP-immunopositivity in the optic nerves were examined, and the amount of H_2S-producing enzyme cystathionine β-synthase (CBS) was estimated using western blotting, ELISA immunoassay, and immunohistochemical (IHC) labeling of CBS in the rainbow trout brain.

Materials and Methods

Animals

Seventy adult male rainbow trout (*Oncorhynchus mykiss*), aged 2.5–3 years, with a body length of 37–45 cm and weighing 370–455 g, were obtained from the Ryazanovka Fish Hatchery (Prymorsky region, Russia). The animals were kept in tanks with a water temperature of 16–17°C with a 14/10-hour light/dark cycle and fed once a day. The dissolved oxygen content of the water was 7–10 mg/dm^3, which corresponds to a normal level. All experimental manipulations with the animals were carried out in accordance with the rules established by the A.V. Zhirmunsky National Scientific Center of Marine Biology (NSCMB), Far Eastern Branch, Russian Academy of Science (FEB RAS), and approved by the Commission on Biomedical Ethics, NSCMB FEB RAS (approval No. 1) on July 31, 2019. The fish were anesthetized by placing in 0.1% solution of tricaine methanesulfonate MS222 (Sigma, St. Louis, MO, USA) for 10–15 minutes.

Mechanical injury of the right eye

The mechanical injury of the right eye was inflicted in accordance with the previously described method (Pushchina et al., 2016a, b, 2018). Using a sterile needle (Carl Zeiss, Oberkochen, Germany), a mechanical damaging impact was applied to the eye area to a depth of 1 cm, with damaging the cornea and mucous membrane of the eye, the retina, the

lens, and the head of the optic nerve with the adjacent tissues. The changes in the histological structure of the adjacent oculomotor muscle fibers, the data of IHCs of PCNA labeling in optic nerve cells, as well as the identification of cells with signs of apoptosis in the damaged optic nerve, indicating a change in its structure due to mechanical injury, were discussed previously (Pushchina et al., 2016a). As a result of the traumatic impact, the central part of the retina, the retinal pigment epithelium, the head of the optic nerve with the oculotomy of the eye muscles (Pushchina et al., 2016b) were damaged. The contralateral optic nerve was used as a control. Immediately after inflicting the mechanical damage, the animals were released into a tank with fresh water for recovery and further monitoring.

Tissue sample preparation for IHC study

After anesthesia, a 0.1 M phosphate buffer (pH 7.2) containing 4% paraformaldehyde solution was injected into the intracranial cavity of the immobilized animals. After prefixation, the brain was removed from the intracranial cavity and fixed in a paraformaldehyde solution at 4°C for 2 hours. The brain was then washed five times in a 30% sucrose solution at 4°C for 48 hours for cryoprotection. Serial frontal and transversal sections of the brain were cut on a Cryo-Star HM 560 MV freezing microtome (Carl Zeiss).

Immunohistochemistry

To study localization of glial fibrillary acidic protein (GFAP, marker for glial cells) in the optic nerve and H_2S-producing cells and fibers (CBS-labeled) in the telencephalon, optic tectum, and cerebellum of the rainbow trout brain, immunoperoxidase labeling of frozen free-floating sections of the optic nerve and brain was used. Activity of GFAP and CBS (marker for H_2S-producing cells and fibers in the brain) was assessed at 1 week after UEI.

The 50-μm thick frozen sections of the ipsi- and contralateral optic nerves were incubated with primary mouse monoclonal anti-GFAP antibodies (GF5 Cat# ab10062; Abcam, Cambridge, UK, dilution 1: 300) at 4°C for 48 hours. A standard ABC complex (Vectastain, Elite ABC kit, Vector Labs, Burlingame, CA, USA) was used to visualize IHC labeling in accordance with the manufacturer's recommendations. To identify the reaction product, a red substrate was used (VIP Substrate Kit, Vector Labs) in combination with methyl green (MG) staining.

To identify H_2S-producing cells and fibers in the telencephalon, optic tectum, and cerebellum of rainbow trout, we used the method of indirect streptavidin-biotin-peroxidase (ABC method) immunolabeling of free-floating sections (Pushchina et al., 2011). CBS immunolabeling occurred in both intact animals and those at 1 week after UEI. The brains of five intact animals and five animals subjected to UEI were fixed in 4% paraformaldehyde solution prepared in a 0.1 M phosphate buffer solution (pH 7.2) for 2 hours at 4°C. The material was washed for 1 day in a 30% sucrose solution and cut into 50-μm-thick sections on a freezing microtome (Cryo-star HM 560 MV; Carl Zeiss). To block the activity of endogenous peroxidase, the sections were incubated in a 1% hydrogen peroxide solution in the 0.1 M phosphate buffer for 30 minutes. The brain sections were incubated *in situ* with rabbit polyclonal antibodies against CBS (GeneTex, Alton Pkwy Irvine, CA, USA; Cat# GTX124346) at a dilution of 1:300 at 4°C for 48 hours. Then the sections were incubated with secondary ready-to-use biotinylated donkey antibodies against rabbit immunoglobulins (ready-to-use; Vector Labs) for 2 hours at room temperature and washed three times with the 0.1 M phosphate buffer for 5 minutes. IHC reaction was demonstrated using a standard rabbit streptavidin-biotin imaging system (HRP conjugated anti-rabbit IgG SABC Kit; Boster Biological Technology, Pleasanton, CA, USA; Cat# SA1022). To identify the products of IHC reaction, the sections were incubated in a substrate to detect peroxidase (VIP Substrate Kit, Vector Labs); for monitoring the color development process under a microscope, the sections were washed and mounted on slides, dehydrated according to the standard protocol, and placed in the BioOptica medium (ZytoVision GmbH, Milano, Italy).

To assess specificity of the immunohistochemical reaction, the negative control method was used. The brain sections were incubated with 1% solution of non-immune horse serum, instead of primary antibodies, for 1 day and processed as sections with primary antibodies. In all the control experiments, no immunoreactivity was detected.

For a comparative analysis of intensity of CBS labeling in the brain of fish from the control group and after UEI, we measured the optical density of CBS-labeled IHC products. The optical density was measured using the Axiovision software (Carl Zeiss) supplied with an Axiovert Apotome 200M inverted microscope. Based on densitometric data, various levels of CBS activity in cells were determined. These data, along with the morphometric parameters of the cells (dimensional characteristics of cell body), were used to classify and typify cells newly formed during the reparative period in the proliferative zones, as well as the definitive brain centers. Optical density (OD) in CBS^+ cells was categorized by the following scale: high (160–120 units of optical density (UOD), corresponding to +++), moderate (120–80 UOD, corresponding to ++), weak (80–40 UOD, corresponding to +), and low (less than 40 UOD, corresponding to –); the initial OD value was measured on the control mounts.

CBS immunosorbent assay

After UEI, the level of CBS in the brain was quantitatively determined using a commercial kit (MBS 7243687; Mir Biotech, San Diego, CA, USA). The ELISA analysis was conducted for tissues from 25 intact rainbow trout and 25 fish with UEI. The brain was removed from the skull in a 0.02 M phosphate buffer, weighed, and thoroughly washed in the ice-cooled 0.02 M phosphate buffer (pH 7.2) to remove blood. Then the brain tissue was mechanically cut into small pieces in 5 mL of phosphate buffer on ice using a glass homogenizer [Potter-Elvehjem polytetrafluoroathylene (PTFE); Sigma]. The rainbow trout brain homogenates contained 10 mg tissue per 100 μL of PBS. The resulting suspension was

subjected to ultrasonic treatment using a sonicator (Sonoplus 2070; Bandelin, Berlin, Germany) to destroy cell membranes. Then the homogenates were centrifuged for 15 minutes at 1500 × *g* on a rotor (Beckman Coulter Ti50, Palo Alto, CA, USA). The supernatant was analyzed using the CBS ELISA Kit (MBS, San-Diego, CA, USA) according to the manufacturer's protocol.

The analysis was performed in a proprietary 96-well microtiter plate. CBS concentration was expressed as pg/mL protein and estimated using a standard curve. The intra- and inter-assay coefficients of variation were lower than 10%. The optical density was measured with a densitometer (Microelisa Stripplate Reader, Bio-Rad, Hercules, CA, USA) at a wavelength of 450 nm for 15 minutes. The assay cross reactivity with other related enzymes was lower than 3%, and the assay sensitivity was 3.6 pg/mL.

Western blot analysis

For western blot analysis, 10 intact adult rainbow trout and 10 fish with UEI were used. The damaged and contralateral optic nerves were removed by separating the fibers of the optic nerves from the adjacent tissues and placed in a 0.01 M Tris-HCl buffer (pH 7.2). The brains of the animals were removed from the skulls in the 0.01 M Tris-HCl buffer (pH 7.2). The optic nerve and brain samples were rapidly cooled and homogenized in triplicate volumes of an ice-cold buffer on a Potter-Elvehim PTFE glass homogenizer (Sigma).

The homogenization buffer contained 20 mM Tris-HCl buffer (pH 7.2) with the addition of 0.25 M sucrose, 10 mM EGTA, 2 mM EDTA, and protease inhibitors: 2 mM PMSF, 50 mg/mL leupeptin, 25 mg/mL aprotinin, 10 mg/mL pepstatin, and 2 mM dithiothreitol. The rainbow trout brain homogenates were centrifuged for 15 minutes at 15,000 × *g* on a Beckman Coulter Ti50 rotor. A 50-mg aliquot of the homogenate was applied to the protein lane and separated using sodium dodecyl sulfate in polyacrylamide-gel electrophoresis (SDS PAGE) on a 10% polyacrylamide gel. After electrophoresis, the isolated protein was accurately transferred to a nitrocellulose membrane and left overnight in a 0.01 M Tris-HCl buffer (pH 8.0) supplemented with a 0.15 M NaCl solution containing 4% BSA (Sigma). The membranes were washed in distilled water and incubated with mouse primary monoclonal anti-GFAP antibodies (GF5 Cat# ab10062; Abcam; dilution 1:300) and rabbit polyclonal anti-CBS antibodies (GeneTex; Cat# GTX124346; dilution 1:300) in the 0.01 M Tris-HCl buffer containing 1% BSA and 0.2% Tween-20 for 3 hours at room temperature. The membranes were then washed with shaking in the 0.01 M Tris-HCl buffer containing 0.2% Tween-20 and incubated with horse anti-mouse secondary antibodies (Vector Labs) or biotinylated donkey antibodies (goat-anti-mouse IgG secondary antibody HRP; Cat# HAF007; Novus Biologicals, Littleton, CO, USA) in the same buffer for 1 hour at room temperature. After washing three times for 10 minutes each, the membranes were placed in the 0.01 M Tris-HCl buffer (pH 7.2).

The immunocytochemical reaction was demonstrated using an ABC avidin-biotin imaging system (Vectastain Elite ABC Kit, Vector Labs) and a streptavidin-biotin imaging system (HRP conjugated anti-rabbit IgG SABC Kit; Cat# SA1022; Boster Biological Technology). To identify reaction product, a red substrate was used (VIP Substrate Kit, Cat# SK-4600; Vector Labs). After color development, the membranes were washed in distilled water and dried. For quantification, the obtained blots were scanned using a Bio-Rad GS 670 densitometer (Microelisa Stripplate Reader, Bio-Rad, Hercules, CA, USA).

Protein concentration in samples was determined in accordance with the method of Bradford (1976) taking BSA as a standard. The method was based on the shift of the absorption spectrum of the Coomassie blue dye G-250 towards 595 nm when it was bound to a protein. To prepare the dye, 10 mg of Coomassie blue G-250 was dissolved with vigorous stirring in 5 mL of 95% ethanol and mixed with 10 mL of 85% phosphoric acid. The mixture was adjusted to 100 mL of H_2O and filtered to remove insoluble dye. Protein concentration in the samples was determined in three analytical replicates. To build a calibration graph, solutions (5–100 μg/mL) were prepared from a standard BSA solution. 1 mL of each sample or BSA calibration solution was mixed with 1 mL of Coomassie blue dye G-250 (Thermo Fisher Scientific, Waltham, MA, USA). The samples were kept in the dark at room temperature for 20 minutes. The optical density of the samples contained in 1 mL glass cuvette was measured with a densitometer (Microelisa Stripplate Reader, Bio-Rad, Hercules, CA, USA) at a wavelength of 595 nm. The protein concentration (mg/mL) of the sample was calculated using the data of the calibration graph.

The molecular weight of GFAP was compared with prestained molecular weight markers (Sigma); it corresponded to the 50 kDa protein isoform. The molecular weight of CBS containing 551 amino acid residues was compared with prestained molecular weight markers (Sigma); it corresponded to 63 kDa. The concentration of GFAP in the optic nerves and the concentration of CBS in the brain homogenates were determined.

Morphometric analysis

Morphometric processing was carried out using an Axiovert 200 M inverted microscope equipped with an ApoTome module and Axio Cam MRM and Axio Cam HRC digital cameras (Carl Zeiss). The measurements were carried out at a magnification of 200×, 400×, and 630× in five randomly chosen fields of view for each area examined.

Statistical analysis

A scheme of animal grouping and experimental design are shown in **Additional Figure 1**. The morphometric data of IHC labeling of GFAP and CBS were quantitatively processed using the STATA statistical software (StataCorp. 2012; Stata Statistical Software: Release 12; StataCorp LP, College Station, TX, USA) and Microsoft Excel 2010 (Microsoft Office Professional E435-2642, Moscow, Russian Federation). All data, expressed as the mean ± SD, were analyzed with the SPSS software (version 16.0; SPSS, Chicago, IL, USA). All

variables measured in the groups were compared using the Student's *t*-test or one-way analysis of variance (ANOVA) followed by the Student-Newman-Keuls *post hoc* test. Values at $P < 0.05$ and $P < 0.01$ were considered statistically significant.

Results

GFAP immunoreactivity in rainbow trout optic nerves

A protein band corresponding to a molecular weight of 50 kDa was observed in the intact optic nerve and in the damaged optic nerve within 1 week after UEI (**Figure 1A**). No heavy protein isoform corresponding to a molecular weight of 90 kDa was detected in the damaged and contralateral rainbow trout nerves. The qualitative content of GFAP in the damaged optic nerve increased compared to the protein content on the contralateral side (**Figure 1A**).

The number of $GFAP^+$ cells and fibers in the damaged and contralateral optic nerves was counted. IHC GFAP labeling was detected in nuclei, as well as in four cell types, whose morphological parameters are provided in **Additional Table 1**. According to the results of the study, GFAP expression was detected in nuclei and morphologically heterogeneous cells, which were divided into four main groups (**Additional Table 1**). Among GFAP-immunopositive cells, we found small rounded cells, corresponding to astroblasts, medium-sized oval cells and elongated, larger ones, corresponding to astrocytes, as well as narrow bipolar cells of all sizes, corresponding to the population of activated astrocytes (Parilla et al., 2009).

A general view of the GFAP-labeled contralateral nerve is shown in **Figure 1B**. In the central part of the nerve, few $GFAP^+$ cells were detected; the distribution density of $GFAP^+$ fibers and cells in the peripheral area of the nerve was higher than that in the central part of the nerve (**Figure 1B**). The distribution of $GFAP^+$ cells and fibers was studied in several neuroanatomical areas of the optic nerve: the head (ONH), the proximal part (PP), the intraorbital segment (IOS), and the distal part (DP) of the nerve before entering the optical tract.

The results of a quantitative analysis of the $GFAP^+$ cell distribution in the contralateral nerve are presented in **Figure 2A**. The largest number of $GFAP^+$ cells and fibers was detected in the ONH (F**igure 2A**), where the distribution density of thick, intensely $GFAP^+$ fibers was also the highest (**Figures 1C** and **2D**).

GFAP- elements in the contralateral optic nerve were represented by large nuclei forming clusters in the peripheral zone of the nerve (**Figure 1D**), as well as by a population of medium-sized oval cells and more elongated cells (**Additional Table 1**). The highest distribution density of $GFAP^-$ cells and nuclei was detected in the IOS of the contralateral nerve; in the ONH, PP, and DP, their concentrations were lower and almost similar (**Figure 2A**).

The distribution of $GFAP^+$ fibers in the contralateral nerve after the eye injury was distinguished by high specificity. The densest and most uniform patterns of distribution were characteristic for IOS (**Figures 1D** and **2D**). In the PP and DP, a cluster pattern of distribution was more common, with groups of labeled fibers and cells identified there (**Figure 1E** and **F**). The lowest density of $GFAP^+$ fibers was found in the DP (**Figure 1F**). Here, large, intensely GFAP-labeled bipolar or rod-shaped cells (**Figure 1F**), representing a population of activated astrocytes, were identified. Unlike oval and elongated fibrous astrocytes, which represent the majority of $GFAP^+$ cells in intact animals, activated astrocytes appeared in the rainbow trout optic nerve only as a result of UEI.

In the damaged optic nerve, we revealed patterns of mass migration of $GFAP^-$ cells from peripheral area of the optic nerve directly to the damage site, which was often accompanied by extended zones of coagulated necrosis expressed to varying degrees (**Figure 3A**). In the peripheral area of the damaged optic nerve, groups of densely GFAP-labeled cells and areas of densely labeled fibers were frequently identified (**Figure 3A**). In the IOS of the damaged optic nerve, extensive regions were occupied by migrating $GFAP^+$ reactive astrocytes distributed along the fibers of the damaged nerve together with the $GFAP^+$ fibers (**Figure 3B** and **E**). In the PP, the distribution density of $GFAP^-$ cells on the periphery of and deep in the ON was relatively high (**Figure 3C**). A significant number of $GFAP^+$ fibers and a relatively low number of $GFAP^+$ astrocytes were characteristic of PP (**Figures 2B**, **2D** and **3C**). In the ONH of the damaged nerve, a large number of medium-sized, oval, and elongated $GFAP^+$ astrocytes and small fragments of $GFAP^+$ degenerating fibers were observed (**Figure 3D**). A large numbers of $GFAP^-$ cells and nuclei were also present in the ONH of the damaged nerve (**Figure 3D**). In the DP of the damaged nerve, mass accumulation of $GFAP^+$ astrocytes of various sizes located along the $GFAP^+$ fibers (**Figure 3F**). The density of distribution of $GFAP^+$ cells in the ONH of the damaged nerve was significantly higher than that in the contralateral nerve ($P < 0.001$). The distribution of $GFAP^+$ astrocytes in the IOS on the damaged side was significantly different from that on the intact side ($P < 0.05$) (**Figure 2C**). The distribution density of $GFAP^+$ fibers in the damaged nerve was significantly higher than that on the contralateral side ($P < 0.05$; **Figure 2D**).

CBS concentration in rainbow trout brain

According to the enzyme immunoassay (**Figure 4A**), CBS concentration was 1.86 ± 0.03 pg/mL in control rainbow trout brain and 3.12 ± 0.26 pg/mL in fish with UEI ($P < 0.001$). Within 1 week after UEI, the concentration of CBS increased 1.7-fold compared to that in the control animals. Western blot assay of CBS concentration in the rainbow trout brain showed the presence of a protein with a molecular weight of 63 kDa. The concentration of CBS in the brain of intact rainbow trout and UEI rainbow trout are shown in **Figure 4B**.

CBS immunoreactivity in rainbow trout brain

Telencephalon of intact trout

The IHC labeling results of CBS in the intact trout telencephalon showed the presence of intensely and moderately labeled cells (**Figure 5A**). In the intact animals, CBS-labeled RG cells were observed in the medial, dorsal, and lateral parts of the pallium (**Figure 5B**, **D** and **F**).

Most of the cells in the dorso-medial region (Dm) were CBS-negative (**Figure 5A**). Intensive CBS labeling was detected in the cells of the periventricular region of the Dm (**Figure 5A**). In the subventricular zone of the Dm, there were clusters of CBS^+ cells; in the deeper layers, only small groups of CBS^+ cells were detected (**Figure 5A** and **B**). In the Dm, two size groups of oval, intensely and moderately labeled CBS^+ cells were identified (**Figure 5B** and **Additional Table 2**). The number of intensely and moderately labeled cells was 46 ± 4/visual filed and 73 ± 6/visual field (**Figure 7A**). In the dorso-dorsal region of the telencephlon (Dd), there were two types of intensively labeled CBS^+ cells: small undifferentiated, located mainly in the periventricular zone (PVZ), and oval, located in the deeper layers (**Figure 5C** and **Additional Table 2**). The RG fibers in the Dd had a high distribution density (**Figure 5D**). The number of undifferentiated cells in the Dd was 35 ± 4/visual field and that of oval cells was 8/visual field (**Figure 7C**). In the dorsolateral region (Dl), the pattern of distribution of RG corresponded to other dorsal areas, with the density of RG distribution being the maximum (**Figure 5E**). In the Dl, two types of CBS^+ cells were also observed (**Additional Table 2**): undifferentiated and oval (**Figure 5F**). The morphometric parameters of CBS^+ cells in the Dl were specific (**Additional Table 2**). The number of intensively labeled undifferentiated cells per visual field was 28 ± 3/visual field; oval, 21 ± 2.4/visual field; moderately labeled, 54 ± 6/visual field (**Figure 7A**). At the border between Dd and Dl, the ratio of CBS^+ cells and RG was as high as possible. In the central part of the dorsal region (Dc), CBS^+ cells were similar to those in the other zones (**Figure 5G** and **Additional Table 2**), but small undifferentiated cells prevailed. The average number of undifferentiated intensely labeled cells in the Dc was 105 ± 8/visual field; oval, 22 ± 3/visual filed; moderately labeled oval cells, 15 ± 3/visual field (**Figure 7A**).

In the subpallial zone of the telencephalon, CBS^+ cells were detected in the medial (Vm) and lateral (Vl) ventral regions (**Figure 5H**). In the Vl, intensely labeled CBS^+ cells were found in the dorsal part (**Figure 5H**) and in the Dl/Vl junction region (data not shown in **Figure 5**). Intensely labeled undifferentiated cells were located in the PVZ (**Additional Table 2**) and oval cells were located deep in the Vl (**Figure 5H**). Larger oval cells were moderately CBS-labeled (**Additional Table 2**). The number of intensely labeled cells was 37 ± 4/visual field, and the number of moderately labeled cells was 74 ± 6/visual field (**Figure 7A**). In the Vm region, CBS^+ cells formed several intensively and moderately labeled discrete groups located along the ventro-lateral telencephalic tract (**Figure 5H** and **I**). Undifferentiated and oval cells were present in the labeled groups (**Additional Table 2**). In the Vm, the number of intensely labeled cells was 73 ± 7/visual field and that of moderately labeled cells was 50 ± 4.6/visual field.

Rainbow trout telencephalon after UEI

In the Dd, intensely and moderately CBS-labeled cells were localized in the PVZ (**Figure 6A**). In this area, a population of undifferentiated cells (**Additional Table 2**) absent in intact animals was identified. Larger CBS^+ oval cells (**Additional Table 2**), not found in intact animals, (**Figure 6B**) appeared in the PVZ. The number of intensely and moderately CBS-labeled cells after UEI increased significantly: 83 ± 7 and 99 ± 8, respectively (**Figure 7B**). In the Dd of the subventricular zone, the number of intensely CBS-labeled oval cells was higher compared with the control (**Figure 6C**). The patterns of localization of moderately labeled differentiated neurons were found to form areas of increased distribution density (**Figure 6D**). After UEI, CBS immunolabeling of some cells was homogeneous, moderate or high; however, the colocalization patterns of intensely labeled cells, with a soma size of approximately 8 μm and with larger moderately or weakly labeled neurons, were observed quite often (**Figure 6B–D**).

In the Dm, the pattern of distribution of immunolabeled cells in the PVZ was similar to that in the Dd (**Figure 6E**); however, intensely labeled single undifferentiated cells and their clusters that are absent in intact animals (**Figure 6E** and **F**, and **Additional Table 2**) appeared in the SVZ. These cells were often located in pairs (**Figure 6F**). The number of intensely and moderately labeled CBS^+ cells in the Dm increased significantly compared with the control animals (**Figure 7B**). In the deeper layers of the Dm, dense clusters of intensely labeled oval cells were detected (**Figure 6G**). Intensely labeled heterogeneous groups of cells (**Figure 6G**) typically appeared in the PVZ. Large reactive neurogenic niches (RNN) with a heterogeneous cell composition were also found here (**Figure 6H**). Most cells in the RNN were CBS^-; they formed a dense central part. As a part of the RNN, there were also intense and moderately labeled oval cells penetrating the entire RNN. Clusters containing CBS^+ cells (**Figure 6H**) were also adjacent to the RNN.

In the Dl, the number of intensely and moderately labeled cells in the PVZ and SVZ increased significantly (**Figure 6I**); moderately labeled cells prevailed in the deeper layers, with their number being many-fold higher than that in the control animals (**Figure 7B**). PVZ was dominated by intensely labeled oval cells arranged into 1–2 rows (**Figure 6J**). In the SVZ, single negative and intensely labeled cells, as well as a heterogeneous population of moderately labeled cells, were observed (**Figure 6J**). In the deeper layers of Dl, there were reactive neurogenic aggregates with a heterogeneous cell composition, not found in the control animals (**Figure 6J**).

In the Dc, in contrast to the other zones, the number of CBS^+ cells somewhat decreased compared to the intact animals (**Figures 6K**, **7B** and **C**). A characteristic feature of Dc was a large number of CBS^- microglial cells migrating along the RG fibers and forming heterogeneous reactive cell groups, including the oval, intensely and moderately labeled cells (**Figure 6L**). As a result of the injury, an additional type of smaller, intensively CBS-labeled, undifferentiated astrocyte-like cells, not detected in the control animals, appeared in the Dc (**Additional Table 2**).

In the subpallial ventro-medial (Vm) part, large and smaller RNN containing CBS-labeled cells were also found after

injury (**Figure 6M** and **Additional Table 2**). The cellular composition of Vm after UEI was significantly different from that of the intact animals (**Additional Table 2**). Most Vm cells showed moderate CBS labeling; a few cells were intensely CBS-labeled (**Figure 6M**). The number of cells in the Vm after UEI significantly increased (**Figure 7B**). In the PVZ and SVZ, CBS^+ cells were detected in the ventral region adjacent to the dorsal (Vd) nucleus (**Figure 6M**). In the Vd, intensely labeled, small, undifferentiated, and elongated migrating cells were found in the PVZ (**Figure 6N** and **Additional Table 2**). In the ventral (Vv) area, larger, intensely labeled, oval cells were observed in the PVZ and SVZ (**Figure 6N** and **Additional Table 2**). In the lateral zone of the Vl, dense CBS labeling was observed in the PVZ, and clusters containing CBS-labeled, intensely and moderately labeled cells were detected in the SVZ (**Figure 6O** and **Additional Table 2**). In the deeper layers of the Vl, moderately labeled cells prevailed, and small RNNs were also observed (**Figure 6O**). An increased density of distribution of CBS^+ cells forming heterogeneous cell clusters was detected in the SVZ (**Figure 6P**). The number of CBS^+ cells in the Vl significantly increased after UEI compared to that in the control animals (**Figure 7B**).

Thus, in the rainbow trout telencephalon after UEI, along with intensely and moderately labeled single cells, we observed local accumulations of intensively CBS-labeled cells in different regions of the pallial zone, as well as reactive CBS^- neurogenic niches in the subpallial zone. The number of CBS^+ cells increased in almost all areas of the telencephalon (**Figure 7C**), with the largest increase in the number of H_2S-producing cells detected in the Dl, Vl, and Vm ($P < 0.01$) and a less significant increase in Dd ($P < 0.5$). There was no significant difference in CBS^+ cells in the Dm compared with the control group, and a slight decrease in the number of CBS^+ cells was observed in the Dc (**Figure 7C**). The percentage of CBS^+ cells in the control animals and after UEI in different regions of the telencephalon is shown in **Figure 7D**.

Tectum of intact rainbow trout

In the intact optic tectum, CBS labeling was observed in the *stratum marginale* (SM), *pia mater*, and *stratum griseum periventriculare* (SGP) (**Figure 8A** and **B**). In the lateral tectum (TeL) SM, areas containing CBS^+ cells and CBS-negative regions were detected (**Figure 8A**). In the CBS-positive regions, mainly small, intensely labeled, neuroepithelial cells, as well as larger oval cells, were observed (**Additional Table 2**). The quantitative ratio of CBS^+ cells in the MS and *pia mater* , as well as CBS-negative cells stained with methyl green as a part of pia mater in TeL, is shown in **Figure 10A**. The maximum number of CBS^+ cells was detected in TeL, as well as their conglomerates in the *pia mater* (**Figure 10A**). In the medial tectum (TeM) in SM, similar cell types were also found to form more extended zones of CBS positivity (**Figure 8B**, **D**, and **Additional Table 2**). Cells were intensely labeled, devoid of processes, and arranged into 1–2 layers. In the composition of *pia mater*, in the area of TeM and TeL, large heterogeneous clusters of CBS^+ cells were clearly observed (**Figure 8B** and **C** and **Additional Table 2**), with their number, however, being lower than that in the TeL (**Figure 10A**). In the dorsal part of the optic tectum (TeD), the pattern of CBS^+ cell distribution corresponded to that in the TeM (**Figure 8E** and **F**), but in some areas, the distribution of CBS^+ and CBS^- cells in *pia mater* was quite specific (**Figures 8G** and **10A**).

In the rainbow trout tectum, CBS-immunopositive, undifferentiated, and oval cells were observed in the SGP (**Figure 8H**, **I**, and **Additional Table 2**). In the dorsal and medial parts of the tectum, the distribution of CBS^+ cells in the SGP was similar in the lateral part, rostral and caudal thickening of the SGP, corresponding to the periventricular matrix zones, with an increased content of CBS^+ cells (**Figure 8I** and **K**). CBS^+ cells in the thickenings were located under a layer of CBS^-proliferating cells (**Figure 8J**). In the caudal periventricular thickening, the CBS^+ cells formed large clusters, often surrounding large vessels of the tectal vascular plexus (**Figure 8K**). Most fibers of the lateral optic tract were located in the area of the caudal thickening, which included individual CBS^+ cells, as well as their small clusters among the periventricular cells (**Figure 8L**). In the composition of central gray layer (SGC) and periventricular gray and white layer (SGAP), single moderately labeled CBS^+ cells of an undifferentiated phenotype were observed; their morphometric parameters are shown in **Additional Table 2**.

Tectum of rainbow trout after UEI

In the medial tectum (TeM), CBS^+ cells were identified in the stratum griseum centrale (SGC) and the stratum griseum et album, periventriculare (SGAP) at 1 week after UEI (**Figure 9A**). Local CBS-negative RNNs were also observed here (**Figure 9A**). In the periventricular layer after UEI, we observed small aggregations of intensely labeled cells, which were absent in intact animals (**Figure 9A**). In the SGP, CBS^+ cells were intensely and moderately labeled, as well as CBS^+ cells, whose nuclei were stained with methyl green; their quantitative ratios in the medial, dorsal, and lateral parts of the tectum are presented in **Figure 10B**. In the SM, we identified larger RNNs, among which there were single CBS^+ cells and labeled RG fibers (**Figure 9B**). The appearance of CBS^+ RG fibers and additional cell types was characteristic of the inner layers of the tectum, SGC and SGAP (**Figure 9C** and **Additional Table 2**).

In the lateral tectum (TeL), CBS^+ cells in the SGP formed numerous dense clusters (**Figure 9D** and **F**), which originated bundles of labeled radial fibers (**Figure 9D**) that were absent in intact animals. In the SGC and SGAP, accumulations of activated CBS^+ astrocytes were observed (**Figure 9E** and **Additional Table 2**). Along RG fibers, CBS cells of oval shape were observed sometimes forming clusters (**Figure 9E**), often single, located among fibers of the lateral optical tract at the SGAP (**Figure 9F**). The ratio of the number of FG fibers and RNN in various regions of the tectum is shown in **Figure 10C**.

In the dorsal tectum (TeD), a large number of CBS^+ cells appeared in the MS and *stratum opticum* (SO) (**Figure 9G**);

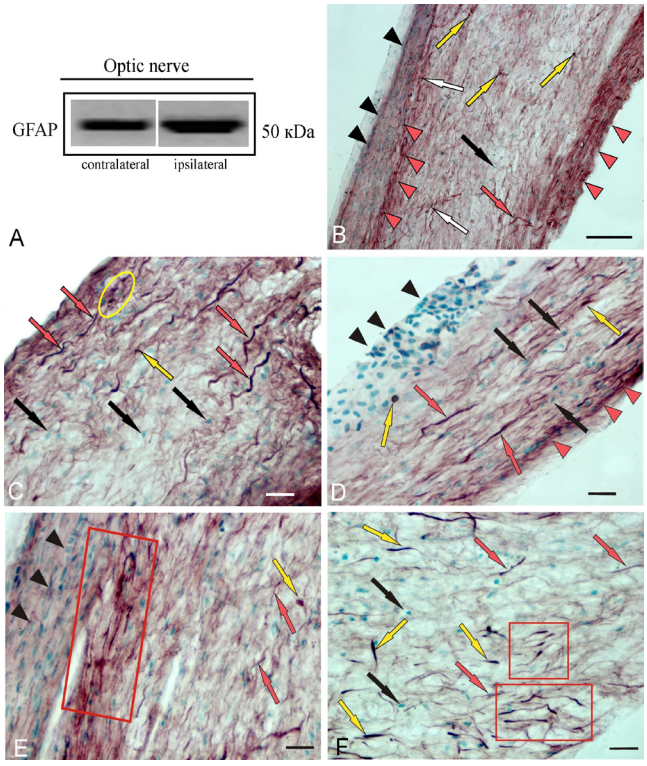

Figure 1 Localization of GFAP in *Oncorhynchus mykiss* at 1 week after unilateral eye injury.
(A) A single protein band corresponding to a molecular weight of 50 kDa in the contra- and ipsilateral nerve. (B) General view of the central part of the contralateral nerve, GFAP$^+$ cells (yellow arrows), nuclei stained with methyl green (black arrows), activated astrocytes (white arrows), GFAP$^+$ fibers (red arrows); black arrowheads indicate clusters of GFAP$^-$ migrated cells; red arrowheads indicate clusters of GFAP$^+$ fibers and activated astrocytes. (C) Optic nerve heads, group of GFAP$^+$ cells (in yellow oval). (D) Intraorbital segment. (E) The proximal part; red box outlines a cluster of GFAP$^+$ cells and fibers; another designations see in A. (F) The distal part of optic nerve; clusters of activated astrocytes are outlined by red boxes; single GFAP$^+$ activated astrocytes are indicated by yellow arrows. Immunoperoxidase labeling of GFAP in combination with methyl green staining. Scale bars: 200 μm in B and 20 μm in C–F. GFAP: Glial fibrillary acidic protein.

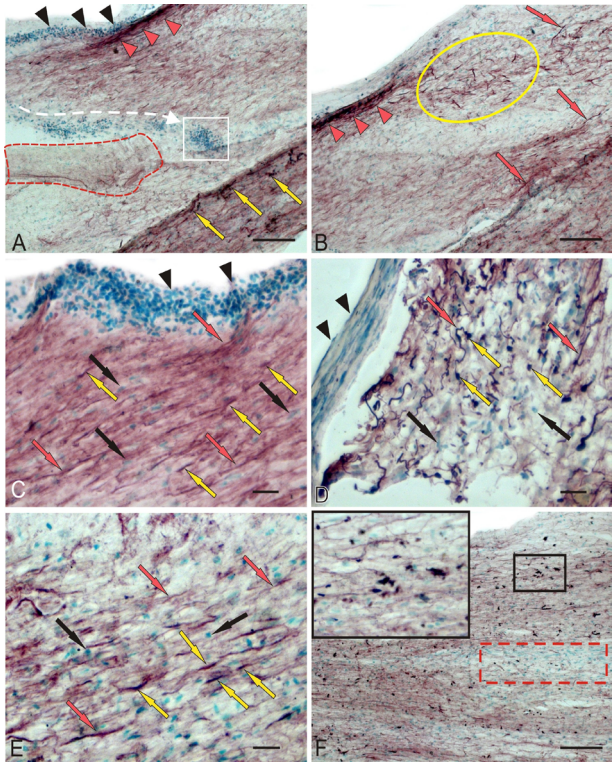

Figure 3 Localization of GFAP in rainbow trout, *Oncorhynchus mykiss*, at 1 week after unilateral eye injury.
(A) The central part of the damaged nerve; black arrowheads indicate clusters of GFAP$^-$ macrophages migrating into the damaged zone (the migration direction is indicated by white dotted lines); in white square, macrophage accumulation; the coagulation necrosis is outlined by red dotted lines; red arrowheads indicate GFAP$^+$ fibers; yellow arrows indicate GFAP$^+$ cells. (B) IOS; a cluster of GFAP$^+$ astrocytes is outlined by yellow oval; separate/single GFAP$^+$ fibers are indicated by red arrows; red arrowheads indicate GFAP$^+$ group of fibers. (C) The proximal part of the damaged nerve; nuclei stained with methyl green are indicated by black arrows; other designations are shown in A and B. (D) ONH. (E) Patterns of GFAP$^+$ and GFAP$^-$ cells in the IOS at higher magnification. (F) Distal part of the damaged nerve; inset (in black boxes) shows an enlarged fragment (original magnification 63×) of the damaged nerve; red dotted line outlines the accumulation of migrating GFAP cells. Immunoperoxidase labeling of GFAP in combination with methyl green staining. Scale bars: 100 μm in A, B, F and 20 μm in C–E and inset in F. GFAP: Glial fibrillary acidic protein; IOS: intraorbital segment; ONH: optic nerve head.

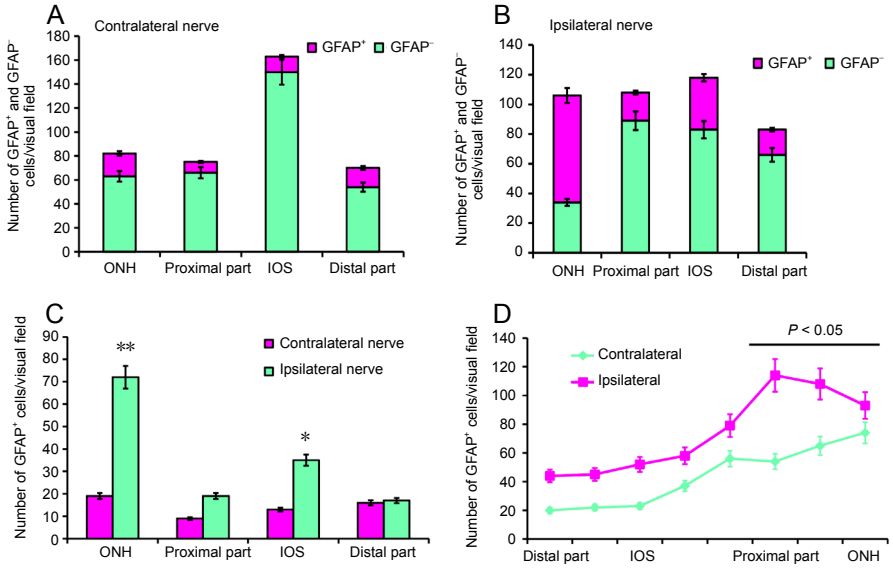

Figure 2 GFAP$^+$ cells and GFAP$^-$ cells on the optic nerves of the rainbow trout, *Oncorhynchus mykiss*, at 1 week after unilateral eye injury.
(A) Number of GFAP$^+$ and GFAP$^-$ cells in the ONH, IOS, proximal and distal parts of the contralateral nerve (mean ± SD). (B) Number of GFAP$^+$and GFAP$^-$ cells on the damaged side (mean ± SD). (C) Number of GFAP$^+$ astrocytes in the contralateral and ipsilateral optic nerves; one-way analysis of variance (ANOVA) followed by the Student-Newman-Keuls *post hoc* test was used to determine significant differences in contralateral and ipsilateral nerves (n = 5 in each group; $*P$ < 0.05, $**P$ < 0.001, *vs.* contralateral optic nerve). (D) Number of GFAP$^+$ fibers in the contralaeral and ipsilateral optic nerves of the rainbow trout; one-way analysis of variance (ANOVA) followed by the Student-Newman-Keuls *post hoc* test was used to determine significant differences between contralateral and ipsilateral nerves (n = 5 in each group; $*P$ < 0.05, *vs.* contralateral optic nerve). GFAP: Glial fibrillary acidic protein; IOS: intraorbital segment; ONH: optic nerve head.

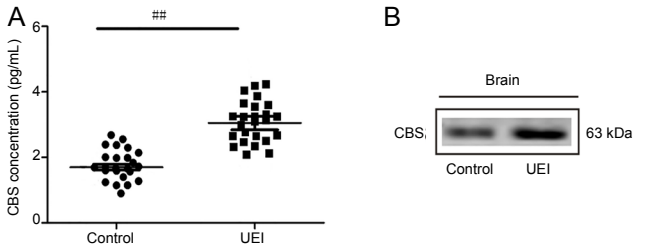

Figure 4 Quantitative analysis of CBS (A) and qualitative demonstration of CBS (B) in the brain of intact rainbow trout and those at 1 week after UEI.

(A) ELISA immunoassay of CBS in the rainbow trout brain at 1 week after UEI *vs.* control (intact) rainbow trout. Student's *t*-test was used to determine significant differences between individuals at 1 week after UEI and control (intact) rainbow trout (##$P < 0.01$); $n = 25$ in each group. (B) A single protein band corresponding to a molecular weight of 63 kDa in the trout brain. CBS: Cystathionine β-synthase; UEI: unilateral eye injury.

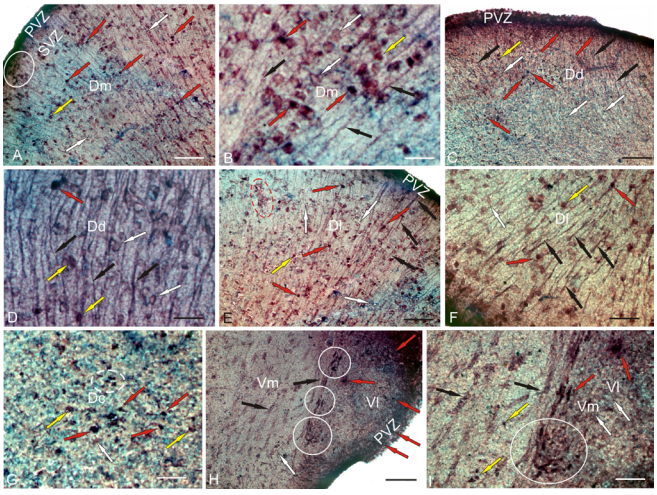

Figure 5 CBS in the telencephalon of the intact rainbow trout *Oncorhynchus mykiss*.

(A) In the dorsal part of the medial area (Dm); intensively labeled cells are indicated by red arrows; moderately labeled cells are indicated by yellow arrows; negative cells are indicated by white arrows; intensively labeled cells are localized in the periventricular zone (PVZ); a cluster of labeled cells in the subventricular zone (SVZ) is outlined by white oval. (B) Dm at higher magnification; black arrows indicate radial glial fibers. (C) In the dorsal part of the dorsal area (Dd). (D) Dd at higher magnification; yellow arrows indicate neuro/glial-like conglomerates labeled in the SVZ. (E) In the dorsal part of the lateral region (Dl): a cluster of weakly and moderately labeled cells is outlined by red dotted line. (F) Dl at higher magnification. (G) In the dorsal zone of the central region (Dc): white dotted line outlines a cluster of intensely labeled cells. (H) In the ventral zone of the medial (Vm) and lateral (Vl) regions: clusters of intensively labeled cells are outlined by white circles. (I) Vm and Vl at higher magnification: a cluster of intensively labeled cells is outlined by white circles. Immunoperoxidase labeling of CBS in combination with methyl green staining. Scale bars: 100 μm in A, C, E, H; 20 μm in B and D; and 50 μm in F, G, I. CBS: Cystathionine β-synthase.

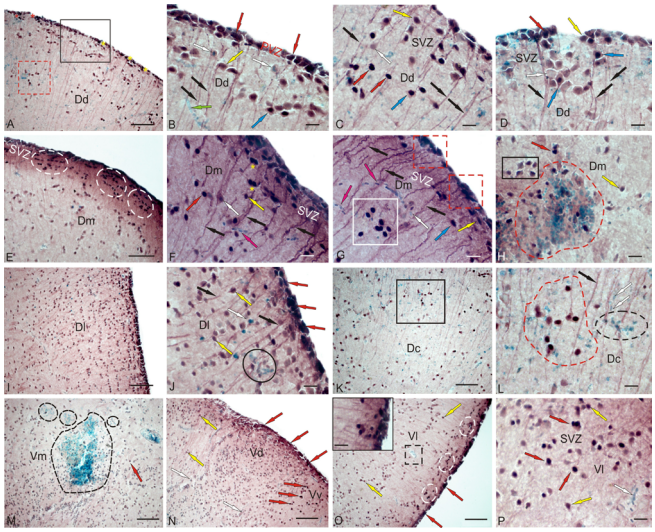

Figure 6 CBS in the telencephalon of rainbow trout *Oncorhynchus mykiss* at 1 week after unilateral eye injury.

(A) Dorsal area (Dd), immunopositive cells in the periventricular zone (PVZ) are outlined by black rectangle; undifferentiated (indicated by red asterisk) and oval (yellow asterisk) cells absent in intact animals; red dotted line outlines a heterogeneous accumulation of CBS^+ and CBS^- cells in the Dd parenchyma. (B) In the PVZ of Dd, at higher magnification; red arrows indicate oval CBS^+ cells in the PVZ; black arrows indicate radial glial fibers, moderately labeled CBS^+ cells are indicated by yellow arrows; negative, by white arrows; blue arrow indicates the neuron/glial-like complexes; green arrow indicates a microvessel. (C) In the subventricular zone (SVZ) of Dd. (D) Patterns of localization of moderately labeled differentiated neurons in the SVZ of Dd, forming areas of increased distribution density. (E) Dm; white dotted lines outline clusters of undifferentiated CBS^+ cells in the SVZ. (F) Dm at higher magnification; paired clusters of undifferentiated CBS^+ cells (yellow stars); CBS^- migrating cells are indicated by pink arrows. (G) Dm, clusters of undifferentiated CBS^+ cells in the PVZ (outlined by red dotted lines); dense accumulation of labeled oval cells in the parenchyma (in white square); (H) reactive neurogenic niche (outlined by the red dotted line) of heterogeneous cell composition in Dm; in black rectangle, a cluster of CBS^+ neurons. (I) Dl with high density of distribution of moderately labeled cells. (J) Dl at a higher magnification; in a black oval, a reactive neurogenic niche. (K) Dc with neuron/glial-like complexes and negative reactive cells (in black square). (L) The fragment in black square in K at higher magnification, in a black cluster of CBS^+ cells, a cluster of CBS^+ cells outlined with red dotted line; immunonegative undifferentiated cells outlined with a black dotted line. (M) Ventral zone of the medial region (Vm), reactive neurogenic niches (circled in black dotted lines). (N) In the ventral zone of dorsal (Vd) and ventral (Vv) nuclei. (O) Ventral zone of the lateral region (Vl); clusters of CBS^+ cells in the SVZ are outlined by white ovals; small reactive neurogenic niche outlined in black dotted lines; heterogeneous accumulation of CBS^+ cells in the PVZ is shown in the inset. (P) Vl at a higher magnification; CBS^+ cells that form heterogeneous cell clusters were identified in the SVZ. Immunoperoxidase labeling of CBS in combination with methyl green staining. Scale bar: 100 μm in A, E, I, K, M–O and 20 μm in B–D, F–H, J, L, P, inset in O. CBS: Cystathionine β-synthase.

some of them were in the state of migration from the surface layers (**Figure 9G**), while others formed RNN. Patterns of cell migration in the TeD were also present in the deeper layers; at the border of SGAP, a layer of intensely labeled oval cells, absent in other parts of the tectum, was observed (**Figure 9G** and **Additional Table 2**). In the SM, small clusters of oval CBS^+ cells were observed (**Figure 9H** and **Additional Table 2**); in some areas, clusters of immunopositive cells were denser (**Figure 9I**), and the intensity of cell labeling in such clusters was very high. In the latero-caudal segment of SGP, large single clusters of intensely labeled cells were localized, with immunonegative RNN observed next to them (**Figure 9J**). In the area of the latero-caudal tectum in the SGC, clusters of tangentially oriented CBS^+ reactive astrocytes were located among CBS- cells (**Figure 9K** and **Additional Table 2**); in some areas of the tectum in the SGC, very large parenchymal RNN were observed (**Figure 9L**). The ratio of CBS^+ cells in different layers of tectum of intact animals and those at 1 week after UEI is shown in **Figure 10D**.

Thus, an essential feature of CBS distribution in intact animals is the intense expression of this enzyme in cells of the neuroepithelial type and cells of *pia mater*, as well as the

periventricular gray layer. H_2S-producing cells of the neuroepithelial type form constitutive clusters in the MS, which are combined with H_2S-negative regions of the tectum. In the inner layers of the tectum, CBS was almost unexpressed, except for single undifferentiated cells with a weak or moderate intensity of CBS labeling. After UEI in the rainbow trout, significant changes in H_2S expression in different cell types occurred in the optic tectum. In general, a multiple increase in CBS expression was observed in the inner layers of the tectum, compared with intact animals. In the MS, the content of CBS^+ cells significantly increased. Along with intensely and moderately labeled single cells, local accumulations of intensely labeled CBS^+ cells in different areas of the tectum, as well as reactive CBS-neurogenic niches were detected. The number of CBS^+ cells in almost all layers of the tectum increased (**Figure 10D**); the largest increase in the number of H_2S-producing cells was detected in the SGC, SGAP, and SGP (**Figure 10D**). The most noteworthy event after UEI is the detection of CBS expression in cells of RG and activated astroglia-like cells, as well as the patterns of radial and tangential cell migration, which are absent in intact animals. The maximum distribution density of the RG was recorded from the lateral part of the tectum (**Figure 10C**).

Cerebellum of intact rainbow trout

In the cerebellum of the intact rainbow trout, CBS expression was detected in different neuroanatomical zones: in the cerebellar body (CCb), granular eminencies (GrE), and the PVZ. CBS labeling was detected in the basal (**Figure 11A**), lateral (**Figure 11B** and **C**), and dorso-medial cells (**Figure 11D**) of CCb. The ratio of CBS^+ cells in the molecular (ML), granular (GrL), and ganglionic layers (GL) of CCb in different parts of the cerebellum is shown in **Figure 13A**.

In the basal and lateral parts of CCb, CBS expression was detected in some types of neurons of the GL: pear-shaped Purkinje cells (PC) and spindle-shaped euryndroid cells (EDC), whose morphological parameters are shown in **Additional Table 2**. In the baso-medial part (BMP), CBS labeling was detected in 38% of PC and 15% EDC, with some of the cells being immunonegative (**Figure 11A**). The ratio of immune and negative PCs, as well as the number of positive EDCs in the BMP, is shown in **Figure 13B**. Separate elongated cells with moderate CBS activity and intensely labeled oval cells were also found in the GrL (**Figure 11A** and **Table 2**). In the ML of the basal part, small, oval, intensely labeled cells were detected (**Figure 11A** and **Additional Table 2**); in some cases, processes of large projection cells and/or ascending fibers (**Figure 11A**) were labeled. The ratio of CBS^+ cells in GL, GrL, and ML to BMP is shown in **Figure 13A**.

In the baso-lateral part (BLP) of CCb, the number of CBS^+ CPs in the GL was lower than in that in the BMP (**Figure 13A**). As a part of GL, PCs were detected in two size groups (**Additional Table 2**), moderately/intensely CBS-labeled, sometimes ectopic into the granular layer in the form of small groups (**Figure 11B**). Small, intensely labeled glia-like cells, also characteristic of BMP, often adjoined moderately labeled PCs (**Figure 11B**, inset). In the ML, intensely labeled small cells were found in the surface layer (**Figure 11B**); undifferentiated small glia-like cells adjacent to negative neurons were observed deep in the ML (**Figure 11B** and **Additional Table 2**). In the GrL, there were few oval CBS^+ cells, moderately/intensely labeled, as well as undifferentiated small, intensively labeled cells, similar to those in the ML and GL (**Additional Table 2**). In the BLP, the number of CBS-negative PCs was significantly higher than that in the BMP; CBS^+ EDCs were not observed in this zone (**Figure 13B**).

In the dorso-lateral part (DLP), the pattern of distribution of CBS^+ cells in the GL was similar to other parts of CCb; however, the number of CBS^+ PCs exceeded that in the basal regions (**Figures 11C** and **13A**). In the DLP, we found the largest labeled PCs with a soma size of 36.6 × 14.9 μm. Bipolar CBS^+ EDCs in the DLP, as well as in the BLP, were not observed, but on the surface of CBS^- EDCs, it was often possible to find small, intensely labeled cells (**Figure 11C**, inset). PCs, as in other parts of CCb, formed two size groups with moderate or high intensity of CBS labeling (**Additional Table 2**). In the GrL, we recorded the greatest diversity of CBS^+ cells, among which were large multipolar poorly labeled neurons, a heterogeneous group of neurons of medium size with moderate or strong labeling intensity, and small oval intensely labeled neurons (**Additional Table 2**). In the ML, two types of intensively labeled cells were identified: oval and small undifferentiated cells (**Additional Table 2**). The number of CBS^+ PCs in the DLP prevailed over CBS^- cells in this zone (**Figure 13B**).

In the dorso-medial part (DMP) of CCb, the number of CBS^+ cells in the GL was lower than that in the DLP; however, larger PCs with moderate labeling intensity dominated this area (**Figures 11D**, **13A**, and **Additional Table 2**). In contrast to the lateral zones (BLP and DLP), DMP contained CBS^+ EDCs; the ratio between CBS^+ and CBS^- PCs was slightly higher than that in BMP (**Figure 13B**). At the apical pole and also in the basal part of the DMP, there was the dorsal matrix zone (DMZ) that contained small intensely labeled cells located bilaterally (**Figure 11D** and **E**). In the GrL, large elongated and smaller oval cells with moderate or high intensity of CBS labeling were observed (**Additional Table 2**). In the ML, small oval intensively labeled cells were observed in the deeper layer (**Figure 11D**, **E**, and **Additional Table 2**). Another type of intensely labeled cells was located on the surface of the layer, at the border with pia matter (**Figure 11D** and **Additional Table 2**). Such cells often formed dense clusters (**Figure 11D**).

In the central part of CCb, two types of CBS^+ cells were observed in the GrL (**Additional Table 2**). The first type included the largest, elongated, moderately labeled cells, on the surface of which numerous small cells and/or terminal apparatus of intensely labeled cells were observed (**Figure 11F**, inset). Among this type, we identified large- and medium-sized cells (**Additional Table 2**). Another type was represented by intensely, uniformly labeled cells, also including a group of oval and small undifferentiated cells (**Figure 11F** and **Additional Table 2**).

In granular eminences (GrE), which are lateral thickenings of the granular layer, numerous CBS^+ cells were observed both in the deep (**Figure 11G**, **J** and **L**) and surface layers (**Figure 11H** and **K**). In the basal part of the GrE, at the border with the brainstem, ascending CBS^+ fibers were detected (**Figure 11I** and **M**). Three types of cells were identified in the GrE; the intensity of CBS labeling ranged from moderate to high (**Additional Table 2**). The first type was represented by large moderately/intensely CBS-labeled multipolar cells (**Additional Table 2**). Another type was represented by oval-shaped neurons of a medium size, which were also labeled moderately or intensely (**Figure 11G** and **J**). The smallest cells in the oval-shaped GrE were intensively labeled (**Additional Table 2**). The quantitative ratio of cells of various types is shown in **Figure 13C**.

As in other areas of the cerebellum, small undifferentiated intensely labeled CBS^+ cells were observed on the surface of GrE (**Figure 11H** and **K**, **Additional Table 2**). Such cells were often grouped into small clusters, or located singly on the surface of GrE (**Figure 11H** and **K**). In the caudal part of GrE, at the border with the *medulla oblongata*, we identified CBS^+ fibers, which are ascending afferents from the inner olivar complex, among which single small, intensely labeled CBS^+ cells were located (**Figure 11I** and **M**). In this area, the pattern of distribution of CBS^+ cells was different from that in the rostral zone (**Figure 11I** and **L**).

Cerebellum of rainbow trout after UEI

After UEI, significant changes in the constitutive patterns of H2S-producing cellular domains occurred in almost all areas of the rainbow trout cerebellum. In the ML of all areas of the cerebellum, a significant increase in the number of CBS^+ cells was recorded (**Figures 12A** and **13C**). In the subsurface layer, we detected clusters containing heterogeneous CBS^+ cells and migrating CBS^+ cells that were absent in the intact animals (**Figure 12B**). Intensely labeled CBS^+ cells absent in intact animals and patterns of mass migration of CBS^+ cells (**Figure 12C** and **Additional Table 2**) were found deep in the ML. In the surface part of the ML, reactivated neurogenic niches of heterogeneous composition, including both CBS-positive and negative cells, were revealed (**Figure 12D**).

Substantial rearrangements of the CBS-producing apparatus (**Figure 12E**) were found in the DMZ after UEI, manifested as a decrease in the number of CBS-immunopositive cells in the DMZ and the intensity of their labeling (**Figure 12F**). At the same time, an intensely labeled group of cells appeared in the surface part of the DMP (**Figure 12G**). Thus, after UEI, there was a change in CBS-immunopositivity of the cells: in the DMZ, CBS expression in the cells decreased; in the surface part of the DML, the induction of CBS in the heterogeneous cell group was absent in intact animals.

An increase in the number of CBS+ EDCs (**Figure 12H**) was recorded and CBS^+ EDCs in the BLP (**Additional Table 2**) appeared in the BMP, with larger cells observed in the basal part of CCb after UEI than in intact animals (**Additional Table 2**). The increase in the number of CBS^+ cells in the GL after UEI is shown in **Figure 13C**. In the deep part of the ML, we found a network of labeled tangential fibers in the BMP, among which CBS-reactive neurogenic niches were localized (**Figure 12I**), and additional types of CBS^+ neurons were also observed (**Additional Table 2**). Unlike intact animals, in the BMP after UEI we observed large, intensely labeled elongated cells (**Figure 12I**), as well as smaller moderately/intensely labeled oval and undifferentiated cells (**Additional Table 2**). In the deep BLP molecular layer, patterns of mass migration of CBS^+ cells were observed (**Figure 12J**). The number of CBS^+ cells increased in the GrL compared with the intact animals (**Figures 12K** and **13C**).

The number of CBS^+ and CBS^- granular cells significantly increased (**Figures 12L** and **13D**) in the GrE, the same as in the GrL. Among the labeled cells, five types with moderate and intensive CBS labeling were observed (**Additional Table 2**). Large multipolar and bipolar cells were weakly labeled (**Figure 12L**). Oval-shaped cells were labeled intensely (**Figure 12L** and **Additional Table 2**). Small, intensely labeled cells were observed both in the periventricular and subventricular layers (**Figure 12M**), where they formed heterogeneous groups, including CBS-labeled and negative cells. In all areas of the GrE, the number of moderately labeled small cells significantly increased compared with the control animals (**Figures 12M**, **N** and **13D**). In the deep layers of the GrE, clusters of labeled oval and small undifferentiated cells in the heterogeneous cell groups were observed (**Figure 12L–O**). In the subventricular zone, we frequently detected reactive cellular domains, including CBS- cells surrounded by moderately and intensely CBS-labeled, small, undifferentiated cells, as well as larger oval intensely labeled neurons (**Figure 12P**). Thus, after UEI in the rainbow trout cerebellum, the number of CBS^+ fibers and cells in different CCb regions increased, the pattern of constitutive expression of CBS in the DMZ changed, CBS in the surface layers of the DMP was detected, cell migration increased, and the number of CBS^+ and CBS- cells in the GrL and GrE increased; in the GrE, heterogenous cell domains containing various types of CBS-producing cells disappeared.

Discussion

Our results showed that the expression of GFAP in the optic nerve and CBS in the integrative centers of the brain had significant differences between intact rainbow trout and those at 1 week after UEI. In all cases, the recorded differences indicate an increased expression of these markers after injury, which indicates the involvement of H_2S in reparative processes.

GFAP expression in intact rainbow trout and those after UEI

The available data on the astroglial cell morphology in the rainbow trout, *Oncorhynchus mykiss*, obtained by GFAP immunohistochemistry, refer only to the cerebellum (Somogyi et al., 1990) and the retina (De Guevara et al., 1994). ICH cross-reactivity between fish and mammalian GFAP is well known in different teleostean: *Cyprinus carpio* (Onteniente et al., 1983; Kálmán, 1998); *Carassius auratus* (Cardone and

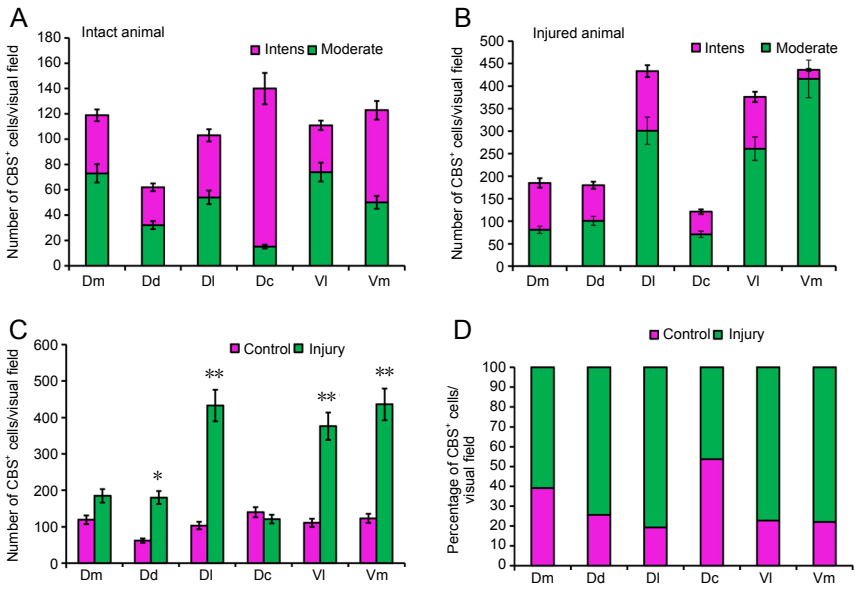

Figure 7 Density of CBS$^+$ cells in the telencephalon of intact rainbow trout *Oncorhynchus mykiss* and those at 1 week after UEI.
(A) The number of intensively and moderately labeled cells in intact animals (mean ± SD). (B) The number of intensively and moderately labeled cells in animals after UEI (mean ± SD). (C) The number of cells in intact rainbow trout and those with UEI. One-way analysis of variance (ANOVA) followed by the Student-Newman-Keuls *post hoc* test was used to determine significant differences in the rainbow trout with UEI and control rainbow trout (n = 5 in each group; $*P < 0.01$, $**P < 0.05$, *vs.* control group). (D) The percentage of labeled cells in intact animals and after UEI. CBS: Cystathionine β-synthase; Dc: dorso-central parts of telencephalon; Dd: dorso-dorsal parts of telencephalon; Dl: dorso-lateral parts of telencephalon; Dm: dorso-medial parts of telencephalon; UEI: unilateral eye injury; Vl: ventro-lateral parts of telencephalon; Vm: ventro-medial parts of telencephalon.

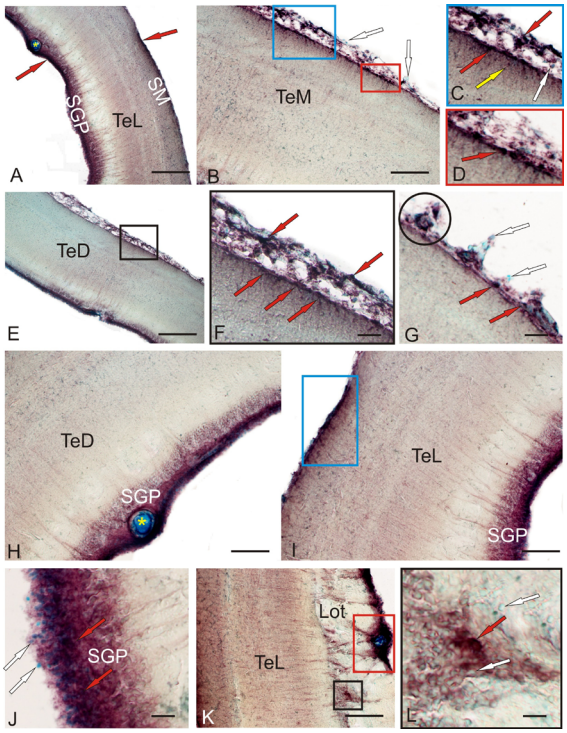

Figure 8 CBS in the optical tectum of an intact rainbow trout *Oncorhynchus mykiss*.
(A) General view of rainbow trout tectum; red arrows indicate accumulations of CBS$^+$ cells in the stratum marginale (SM) and periventricular gray (SGP) layers; yellow star indicates a blood vessel. (B) Medial zone of tectum (TeM); in rectangles are fragments containing CBS$^+$ cells in pia matter (blue rectangle) and radial glia (red and blue rectangles); white arrows indicate immunonegative cells. (C) The fragment in the blue rectangle in B; red arrows indicate superficial CBS$^+$ cells, yellow arrow indicate migrated CBS$^+$ cells, and white arrow indicates CBS-immunonegative cells. (D) The fragment in the red rectangle in B at a higher magnification. (E) Dorsal zone of tectum (TeD); in black square of CBS$^+$ cells in *pia matter* and SM. (F) Inset at E on a higher magnification, red arrows indicate superficial CBS$^+$ cells. (G) Clusters (in black circle) of CBS$^+$ and CBS$^-$ cells in pia matter TeD; red arrows indicate superficial CBS$^+$ cells, white arrows indicate CBS-immunonegative cells. (H) CBS-immunopositive cells in the SGP (in TeD); white star indicates a blood vessel. (I) In the SGP lateral tectum (TeL); blue rectangle outlines a cluster of CBS$^+$ cells in the SM. (J) CBS$^+$ cells in the caudal pole of TeL; red arrows indicate superficial CBS$^+$ cells, white arrows indicate CBS-immunonegative cells. (K) CBS$^+$ cells forming clusters surrounding the main vessels of the tectal choroid plexus (in the red rectangle); ectopic immunopositive cells among the fibers of the lateral optical tract (in black square). (L) Inset of the black square in K at a higher magnification; red arrows indicate superficial CBS$^+$ cells, white arrows indicate CBS-immunonegative cells. Immunoperoxidase labeling of CBS in combination with methyl green staining. Scale bars: 200 μm in A and E, 100 μm in B, H, I, K, and 20 μm in F, G, J, L. Original magnification, 63× in C and D. CBS: Cystathionine β-synthase.

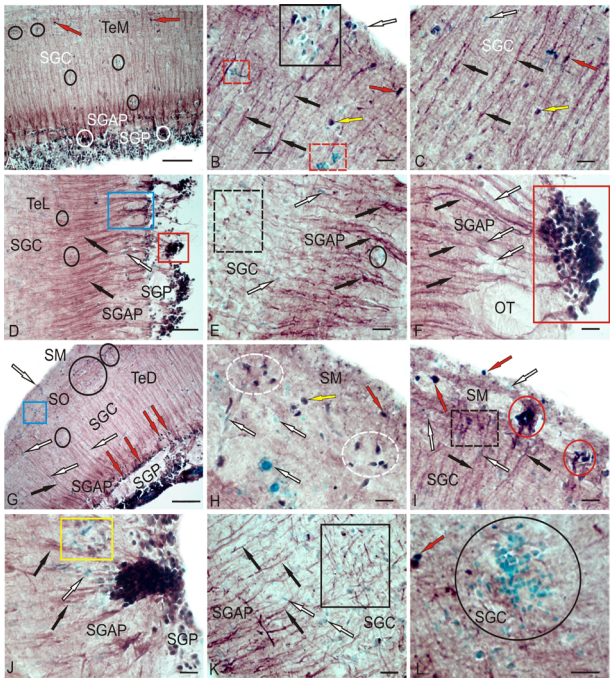

Figure 9 CBS in the optical tectum of rainbow trout *Oncorhynchus mykiss* at 1 week after UEI.
(A) In the medial zone of tectum (TeM); CBS$^+$ cells in the SGC are indicated by red arrows; reactive neurogenic niches (RNN) are outlined by black ovals; and CBS$^+$ cells in the SGP are indicated by white ovals. (B) Large RNN in the stratum marginale (SM) (black square), small RNN (red dotted square), radial fibers (by black arrows), CBS$^-$ cells (white arrow), intensively labeled cells (red arrow), and moderately labeled cells (yellow arrow). (C) CBS$^+$ radial glia fibers (black arrows) in the SGC (other designations see in B). (D) CBS$^+$ cells forming numerous dense clusters in the SGP (in the red rectangle) and bundles of CBS$^+$ radial fibers in the SGAP (in blue rectangle); radial fibers are indicated by black arrows and CBS$^-$ cells are indicated by white arrow). (E) Clusters of activated CBS$^+$ astrocytes (outlined by black dotted line) in the lateral tectum (TeL); reactive neurogenic niches (RNN) are outlined by black oval. (F) CBS$^-$ cells (white arrows) located among fibers of the lateral optical tract; radial fibers (by black arrows), red rectangle outlines a cluster of CBS$^+$ cells at a higher magnification; (G) CBS-migrating cells in the SM (in blue rectangle) and RNN in the SO (in black ovals) of the TeD; (H) Diffuse group of CBS$^+$ cells (in white dotted ovals) in the SM at a higher magnification. (I) Dense cluster of CBS$^+$ cells in the SM (in red ovals); CBS$^+$ radial glia in black dotted rectangle. (J) A large single cluster of CBS$^+$ cells, next to CBS-negative RNN (in yellow rectangle). (K) Clusters of tangentially located CBS$^+$ reactive astrocytes (in black rectangle); L – Large parenchymal RNN (in oval) in the SGC. Immunoperoxidase labeling of CBS in combination with methyl green staining. Scale bars: 100 μm in A, D, G and 20 μm in B, C, E, F, H–L. CBS: Cystathionine β-synthase; RNN: reactive neurogenic niches; SGAP: stratum griseum et album periventriculare; SGC: stratum griseum centrale; SGP: stratum griseum periventriculare; SM: stratum marginale; SO: stratum opticum; TeD: dorsal tectum; UEI: unilateral eye injury.

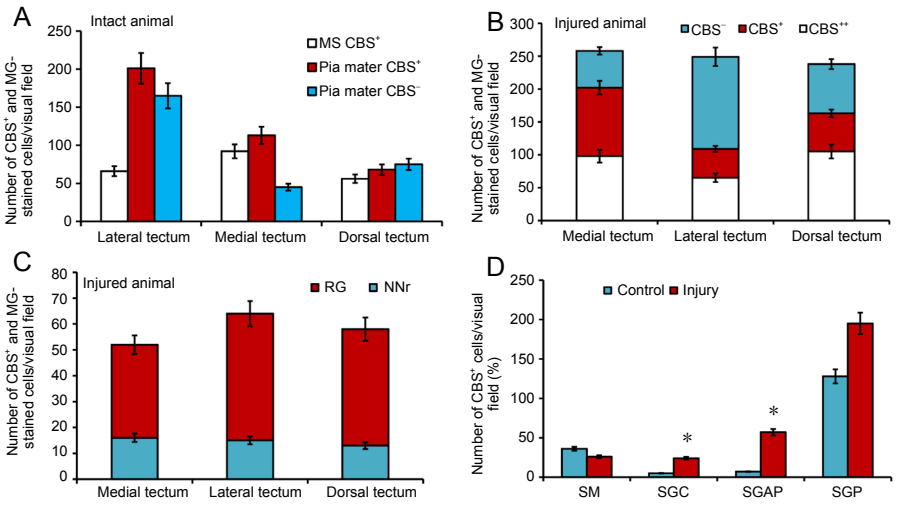

Figure 10 Density of CBS$^+$ cells in the optic tectum of rainbow intact trout *Oncorhynchus mykiss* and those at 1 week after UEI.
(A) The number of intensively, moderately labeled, and MG-stained cells in intact animals in different parts of the tectum (mean ± SD). (B) The number of intensively, moderately labeled, and MG-stained cells in different parts of the tectum after UEI (mean ± SD). (C) The number of radial glia cells (RG) and reactive neurogenic niches (NNr) in different parts of the tectum after UEI (mean ± SD). (D) The number of cells in intact tectal layers and after UEI; one-way analysis of variance (ANOVA), followed by the Student-Newman-Keuls *post hoc* test, was used to determine significant differences in control animals and those subjected to UEI (n = 5 in each group; mean ± SD, $*P < 0.05$, *vs.* control group). CBS: Cystathionine β-synthase; SGAP: *stratum griseum et album periventriculare*; SGC: *stratum griseum centrale*; SGP: *stratum griseum periventriculare*; SM: *stratum marginale*; UEI: unilateral eye injury.

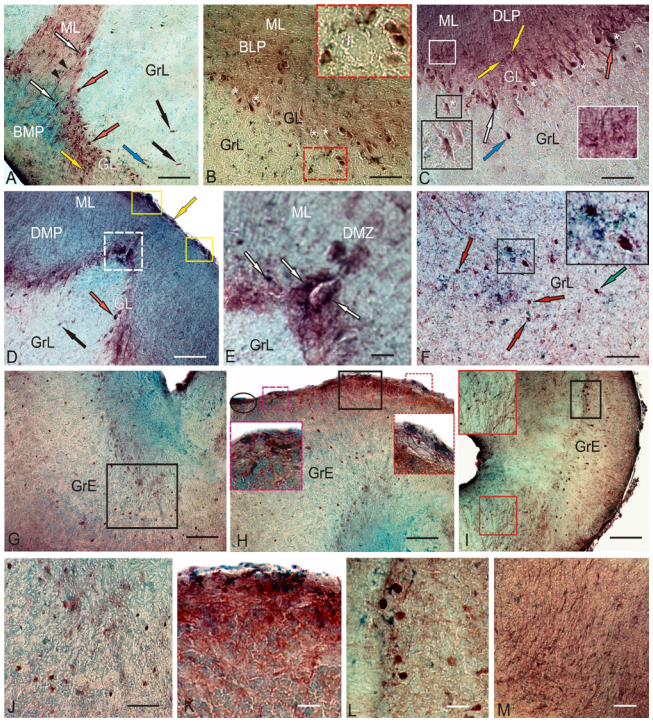

Figure 11 CBS in the cerebellum of the intact rainbow trout *Oncorhynchus mykiss*.
(A) In the BMP, CBS$^+$ Purkinje cells (red arrows), euridendroid cells (white arrows), intensively labeled cells in the GrL (blue arrow) and ML (yellow arrow), moderately labeled cells in the GrL (black arrows), and immunopositive fibers (black arrowheads). (B) In the BLP, CBS$^-$ Purkinje cells (white asterisk), CBS$^+$ Purkinje cells ectopic into a granular layer; a fragment outlined by red dotted line (inset). (C) In the DLP, CBS$^-$ EDC are small, intensively labeled cells (inset in a black rectangle), in a white rectangle (inset) a fragment with CBS$^+$ cells in the ML. (D) In the DMP, CBS$^+$ cells in the surface zone of the ML (in yellow rectangles), and the DMZ (outlined by white dotted line). (E) The DMZ at a higher magnification. (F) The central part of cerebellum in the GrL, elongated CBS$^+$ cells, numerous terminal thickness of intensely labeled cells (inset), and intensely uniformly CBS-labeled cells (green arrow). (G) In the GrE, CBS$^+$ cells in the lateral part (in black rectangle). (H) In the surface layers of the rostral region GrE (inset), red and pink dotted lines delineated insets in large red and pink rectangles. (I) CBS$^+$ fibers and cells at the level of the inner olivar complex (inset in red rectangle), and dorsal group of CBS$^+$ cells (in black rectangle). (J) In the deep part of the GrE. (K) In the surface part of the caudal region GrE. (L) Enlarged fragment in the black rectangle (I). (M) CBS$^+$ fibers of inner olivar complex at a higher magnification. Immunoperoxidase labeling of CBS in combination with methyl green staining. Scale bars: 100 μm in A–D, F, 200 μm in G–I, and 50 μm in E, J–M. BLP: Baso-lateral part of cerebellar body; BMP: baso-medial part of cerebellar body; CBS: cystathionine β-synthase; DLP: dorso-lateral part of cerebellar body; DMP: dorso-medial part of cerebellar body; DMZ: dorsal matrix zone; EDC: euryndroid cells; GrE: granular eminencies; GrL: granular layer; ML: molecular layer.

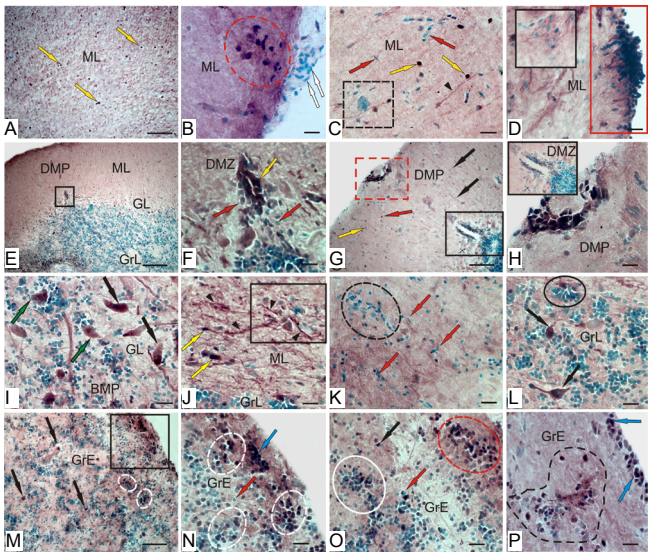

Figure 12 CBS in the cerebellum of rainbow trout *Oncorhynchus mykiss* at 1 week after unilateral eye injury.
(A) CBS$^+$ cells in the ML (yellow arrows). (B) Clusters of CBS$^+$ cells (outlined by red dotted line) and migrating CBS$^-$ cells (white arrows). (C) CBS$^+$ cells in the ML (yellow arrows), patterns of migration of CBS$^-$ cells (red arrows), clusters of CBS$^-$ cells (outlined by black dotted lines), and radial glia fibers (black arrowhead). (D) In the surface part of the ML, reactivated neurogenic niches containing CBS$^+$ cells (red rectangle), and CBS$^-$ cells (black rectangle). (E) A common view of DMP, DMZ in the black square. (F) DMZ at a higher magnification. (G) Additional intensively labeled group of cells in the surface part of the DMP (red dotted line), DMZ in black box. (H) DMP at a higher magnification. (I) Intensively CBS-labeled EDC (black arrows) and moderately labeled (green arrows) cells in the BMP. (J) CBS$^+$ tangential fibers (black arrowheads); CBS$^-$ reactive neurogenic niches (in rectangle). (K) Patterns of migration of CBS$^-$ cells (outlined by black dotted lines). (L) CBS$^+$ cells (black arrows) in the GrE; a cluster of CBS-negative and single positive cells in black oval. (M) CBS$^+$ cell clusters in the surface areas of the GrE (in black square) and inner layers (outlined by white dotted line) of the GrE. (N) GrE surface layers at a higher magnification. (O) GrE inner layers at a higher magnification; heterogeneous cell clusters are outlined by white and red ovals. (P) Reactive cell domains in the subventricular zone (outlined by a dotted line) of the GrE, blue arrows indicate CBS$^+$ cells. Immunoperoxidase labeling of CBS in combination with methyl green staining. Scale bars: 100 μm in A, E, G, M, and 20 μm in B–D, F, H, I–L, N–P. CBS: Cystathionine β-synthase; DMP: dorso-medial part of cerebellar body; DMZ: dorsal matrix zone; GrE: granular eminencies; GrL: granular layer; ML: molecular layer.

Roots, 1990); *Barbus comiza* (Bodega et al., 1993); *Danio rerio* (Marcus and Easter, 1995) and selachian: *Mustelus canis* and *Raja ocellata* (Dahl et al., 1985); *Torpedo marmorata* and *Scyliorhinus canicula* (Wasowicz et al., 1999); *Raia erinacea* and *Squalus acanthias* (Kálmán and Gould, 2001); and in Actinopterygii, chondrostei, *Acipenser ruthenus* (Kálmán and Ari, 2002). According to these reports, GFAP is a conserved protein that may vary in molecular weight during vertebrate phylogenesis.

GFAP expression is characteristic of reactive astrocytes after injury in mammals (García and Koke, 2009) and has been previously described from teleost ON after crush (Parilla et al., 2013). On the other hand, the maintenance of GFAP expression in the ON during fish adulthood seems to be related to the constitutive growth and regeneration processes due to the fact that they confer immature characteristics to the astrocytes and plasticity to the system (Maggs and Scholes, 1990).

The estimation of the number of $GFAP^+$ cells and fibers on the side of the damaged nerve and on the contralateral side showed labeling of GFAP in the nuclei and four cell types. Among $GFAP^+$ cells of the rainbow trout ON, there were small rounded cells, corresponding to astroblasts, oval cells of a medium size and elongated, larger cells, corresponding to astrocytes, as well as narrow bipolar cells of all sizes, corresponding to populations of activated astrocytes according to the classification by Parilla et al. (2009). Depending on their immunoreactivity to the C4 antibody, at least two different types of astroglia have been identified in the mature zebrafish brain (Tomizawa et al., 2000). One of these two glial populations may represent the mature astroglia, and the other may be involved in axon outgrowth or regeneration (Clint and Zupanc, 2001). Distinct glial subpopulations have also been described from lower vertebrates (Margotta and Morelli, 1997; Yoshida, 2001).

The results of a quantitative analysis of the distribution of $GFAP^+$ cells in the contralateral nerve of rainbow trout showed that the largest number of $GFAP^+$ cells and fibers is localized in the ONH. The analysis also revealed the highest distribution density of thick, intensely GFAP-labeled fibers. Another important finding is the identification of large, intensely labeled bipolar cells, representing a population of activated astrocytes that are absent in intact animals, including rainbow trout, and appear in the ON only as a result of injury. Our results also show an increase of GFAP expression in the ON of *O. mykiss* after UEI, which agrees with the data on the goldfish ONH after ON crush (Parilla et al., 2013), supporting the observations from these previous studies. In this region, we also found a source of new astrocytes, PCNA and Pax2 that is activated after injury (Pushchina et al., 2016a, 2018).

In the damaged nerve, patterns of mass migration of $GFAP^-$ cells from peripheral areas of the nerve towards the damage site were observed. In the peripheral areas of the damaged nerve, groups of intensively GFAP-labeled cells and areas of densely labeled fibers were often identified. In IOS of the damaged nerve, vast areas were occupied by migrating $GFAP^+$ reactive astrocytes extending along the fibers of the damaged nerve together with $GFAP^+$ fibers. Expression patterns of GFAP and keratins were described from the goldfish ONH after ON crush (Parilla et al., 2013). We suggest that the maintenance of keratin and GFAP expression in the ON during fish adulthood can be related to the continuous growth and regeneration processes (Druger et al., 1994).

In the proximal part of the rainbow trout nerve, the distribution density of $GFAP^-$ cells on the periphery and deep in the ON was relatively high. The significant amount of $GFAP^+$ fibers and the relatively low levels of $GFAP^+$ astrocytes were characteristic of the proximal part of the optic nerve in rainbow trout. In the ONH of the damaged nerve, we detected a maximum number of medium-sized, oval and elongated astrocytes of medium-sized $GFAP^-$ and small fragments of $GFAP^+$ degenerating fibers. In general, the patterns of distribution of GFAP at 1 week after UEI in rainbow trout were consistent with the data on goldfish with the optic nerve injury (Parrilla et al., 2013).

The distal part of the damaged nerve in rainbow trout was mostly characterized by mass accumulation patterns of $GFAP^+$ astrocytes of various size groups along the $GFAP^+$ fibers. The density of distribution of $GFAP^+$ cells in the ONH damaged nerve was significantly higher than that in the contralateral nerve. In the IOS, significant differences in the distribution of $GFAP^+$ astrocytes were found between the damaged nerve and contralateral nerve. The distribution density of $GFAP^+$ fibers in the damaged nerve significantly exceeded that on the contralateral side.

Finally, a strong reaction of astrocytes surrounding the posterior ONH, which are positive to Pax2, GFAP, and neurolin, was revealed after UEI (Pushchina et al., 2018; Pushchina and Varaksin, 2019). Previously, this astrocyte ring has only been described from the ONH after cryolesion (Parrilla et al., 2012, 2013) and is located in a region similar to *lamina cribosa* in turtle and mammals (Dávila et al., 1987; Fujita et al., 2000). GFAP is a structural protein that confers rigidity and protection to the axons of retinal ganglion cells (Lillo et al., 2002) and forms a part of the fish ONH glia limitans (Lillo et al., 2002; Parrilla et al., 2009).

Expression of CBS in the rainbow trout brain after UEI

The H_2S-producing systems in rainbow trout at 1 week after UEI were studied by enzyme immunoassay, western immunoblotting, and IHC of polyclonal antibodies against CBS in three integrative brain centers: telencephalon, optic tectum, and cerebellum. ELISA results showed a 1.7-fold increase in CBS expression in the rainbow trout brain within 1 week after UEI compared to that in intact animals.

According to Northcutt (2008), fish optic tectum is a region of the brain that receives direct projections from the retina. In this brain region in rainbow trout after UEI, we previously observed reactivation of constitutive neurogenic niches with a heterogeneous cell composition, including $PCNA^+$, $HuCD^+$, $Pax6^+$ cells (Pushchina et al., 2016a, b, 2018; Pushchina and Varaksin, 2019). As centers that lack direct retinal inputs in the rainbow trout brain, we considered the telencephalon and the cerebellum. Studies conducted in var-

ious areas of the fish brain showed the presence of progenitor cells with the properties of neural stem cells (Than-Trong and Bally-Cuif, 2015). Previously, these centers of fish were found to contain RG (Menuet et al., 2005; Ito et al., 2010), which is the main source of long-term constitutively active and/or activated precursors characterized by high heterogeneity, including neuroepithelial progenitors.

Telencephalon

CBS in the pallial and subpallial proliferative zones

The results of IHC CBS labeling in the rainbow trout telencephalon showed the presence of intensely and moderately labeled cells in the pallial and subpallial regions. CBS-labeled cells were located in the superficial periventricular and subventricular pallial layers. In deep pallial areas, particularly in the Dc, the number of intensely labeled cells was higher. The presence of H_2S-producing enzyme in brain cells is associated with the process of neurochemical signaling and, in particular, with the activation of NMDA receptors. The activation of neurons in the vertebrate brain causes the release of neurotransmitters, including glutamate, which activates NMDA receptors, which, in turn, leads to an increase in astrocytic intracellular calcium and long-term potentiation (Nagai et al., 2004; Kimura, 2013). Thus, the presence of two levels of CBS activity in the rainbow trout telencephalon indicates the mediator/modulatory intercellular interactions, which is consistent with the previously obtained data on fish (Pushchina et al., 2011).

It should be noted that the results of the use of polyclonal antibodies against CBS in IHC labeling in the rainbow trout telencephalon are somewhat different from labeling with monoclonal antibodies (Pushchina et al., 2011, 2019; Pushchina and Varaksin, 2011). In intact trout, CBS-labeled RG were observed by labeling with polyclonal antibodies against CBS, particularly in the pallial and subpallial regions of the telencephalon, while labeling with monoclonal antibodies revealed no similar structures (Pushchina et al., 2019). Present data suggest that in the rainbow trout telencephalon, CBS may label adult neural stem cells (aNSCs) with a glial phenotype (RG). Our assumption is consistent with the results of the study of the pallial neurogenic niche in adult zebrafish that contains RG-like NSCs with cellular bodies lining the walls of the ventricle (Cuoghi and Mola, 2009). Studies of the biology of H_2S in the mammalian brain have shown that astrocytes and glial cells are the main repositories of CBS in the brain (Kimura, 2013). *In vitro* studies have shown that astrocytes produce 7–7.5 fold more H_2S than microglial cells (Lee et al., 2009). However, detection of typical astrocytic glia in the fish brain gives controversial results (Arochena et al., 2004; Alunni et al., 2005), and the RG is often found when attempts are made to identify glial architectonics of the brain (Kálmán, 1998).

In the surface layer of different zones of the trout telencephalon, we also identified CBS^+ cells and RG and cells of neuroepithelial type, which are a part of the constitutive matrix zones of the telencephalon. Thus, in the zones of constitutive neurogenesis in the telencephalon of intact animals, CBS^+ cells were detected, which is consistent with the previously obtained data on masu salmon and carp (Pushchina et al., 2011). Studies on *D. rerio* have shown that aNSCs are associated with the ventricular system. In the fish telencephalon, aNSCs have a typical morphology of radial glia and/or neuroepithelium, which can be identified with several molecular markers of aNSCs (Ganz et al., 2010; März et al., 2010). Thus, it is obvious that the CBS^+ cells of the pallial and subpallial regions of the trout telencephalon belong to aNSCs, the neuroepithelial, and glial types. Earlier studies on rainbow trout showed that as a result of UEI in the Dd, Dm, and Dl pallial zones, the number of $PCNA^+$ and $HuCD^+$ cells significantly increases, indicating a significant proliferative and neurogenic activity in the telencephalon (Pushchina et al., 2016a). As a result of UEI, the number of CBS^+ cells in all areas of the telencephalon, except for Dc, increases. The number of H_2S-producing cells increases in the periventricular and subventricular regions of the telencephalon, which are characterized by the intensification of proliferative processes that occur after UEI.

CBS in the telencephalic parenchyma

An increase in the telencephalon parenchyma of another type of intensely labeled CBS^+ cells without processes adjacent to large moderately labeled neurons suggests the intercellular neuron/glial or neuron/microglial interactions associated with the release of H_2S from intensely labeled astrocyte-like cells and/or microglia (Nagai et al., 2004; Hu et al., 2007). In addition, after UEI, the patterns of distribution of CBS^+ RG in the telencephalon are retained, which indicates an additional production of H_2S in aNSCs of the glial type. Studies have shown that after ischemic brain damage, additional production of H_2S is provided by sulfhydration (Kimura et al., 2012). In more recent studies, polysulfides have been shown to be 300 times more active than H_2S in the activation of TRPA1 receptors (Kimura et al., 2013). Polysulfides activate NMDA receptors, which is accompanied by H_2S-dependent reduction of cysteine disulfide in the extracellular domain of the receptor (Kimura, 2013). In this context, activation of NMDA channels by H_2S is probably a detrimental condition arising from the excitotoxicity of glutamate causing calcium influx, which, in turn, leads to neuronal toxicity and cell death (Mark et al., 2001; Wang et al., 2014).

The results of experimental *in vitro* studies have shown that the glutamate toxicity during traumatic injury (ischemia) is weakened by the effect of H_2S on KATP and CFTR Cl^- channels (Kimura, et al., 2006) and activation of GLT1 transporters (Xiao et al., 2012). However, currently there is no consensus on the dual role of H_2S in glutamate toxicity. Neurons that are formed in the matrix PVZs of the trout telencephalon are immature cell forms that migrate from the periventricular to the subventricular layers of the brain. Such non-differentiated cells can express an incomplete set of glutamate NMDA receptors, and, therefore, those cascade processes that trigger apoptosis in mature neurons in immature cells cannot cause death. On the other hand, it is

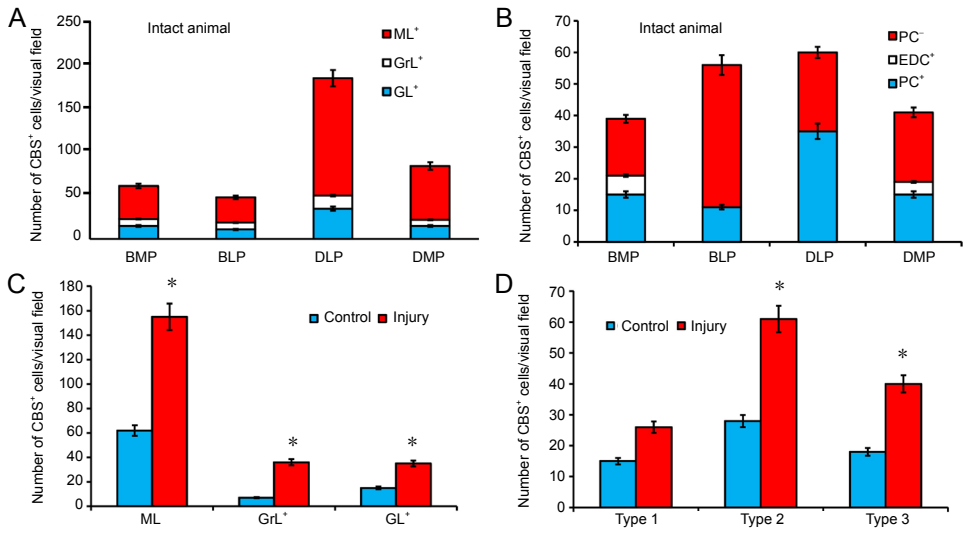

Figure 13 Density of CBS$^+$ cells in the cerebellum of intact rainbow trout *Oncorhynchus mykiss* and those at 1 week after unilateral eye injury.
(A) Ratio of CBS$^+$ cells in the ML, GrL, and GL of CCb in different parts of the cerebellum (mean ± SD). (B) Ratio of PC and EDC in different parts of the cerebellum (mean ± SD). (C) The number of cells in intact cerebellar layers (ML, GrL, and GL) and after unilateral eye injury; one-way analysis of variance (ANOVA), followed by the Student-Newman-Keuls *post hoc* test, was used to determine significant differences in control animals and those after unilateral eye injury (n = 5 in each group; mean ± SD, $*P < 0.05$, *vs.* control group). (D) The number of types 1–3 of cells in intact cerebellum and after UEI; one-way analysis of variance (ANOVA), followed by the Student-Newman-Keuls post hoc test, was used to determine significant differences in control animals and those subjected to unilateral eye injury (n = 5 in each group; mean ± SD, $*P < 0.05$, *vs.* control group). BLP: Baso-lateral part of cerebellar body; BMP: baso-medial part of cerebellar body; CBS: cystathionine β-synthase; CCb: cerebellar body; DLP: dorso-lateral part of cerebellar body; DMP: dorso-medial part of cerebellar body; DMZ: dorsal matrix zone; EDC: euryndroid cells; GL: ganglionic layer; GrE: granular eminencies; GrL: granular layer; ML: molecular layer; PC: Purkinje cells.

known that H_2S is metabolized by mitochondria through the involvement in the oxidation process of H_2S-producing enzymes (Hildebrandt and Grieshaber, 2008; Jiang et al., 2013). The stress-induced H_2S production in mitochondria and the subsequent increase in ATP production have been demonstrated (Fu et al., 2012).

Changes in mitochondrial membrane potential activate caspase-3 and then are attenuated by NaHS in neuronal cell culture, what protects neurons from apoptosis (Luo et al., 2013). Thus, the controversial role of H_2S in mammalian brain neurons raises some questions, such as whether the excessive production of H_2S causes the death of mature neurons in the trout brain as a result of UEI. It is probable that H_2S has a protective effect on the immature telencephalic cells after UEI. What phenotype (glial or neuronal) does correspond to cells that produce H_2S after injury in the trout brain? Considering our previous evidence that the cells of these zones in the rainbow trout telencephalon are HuCD$^+$ (Pushchina et al., 2016a), it is fair to assume that the H_2S-producing cells in the telencephalon of the rainbow trout can represent immature neurons. However, the detection of CBS expression in RG cells indicates a glial phenotype. Thus, it can be concluded that, as a result of UEI in the rainbow trout telencephalon, CBS expression is activated both in the neuronal and glial cell populations.

Optic tectum

In the tectum of an intact trout, we identified zones that contain intensely labeled neuroepithelial cells in SM, alternating with areas lacking immunopositivity. We believe that the surface sites containing CBS immunopositivity correspond to the areas of constitutive neurogenesis in the trout tectum. The volume and extent of such zones containing CBS-immunopositive neuroepithelial cells in the dorsal and medial areas of the tectum exceeded those in the lateral region. Another characteristic feature was the CBS-labeled cells in the pial membrane, where such cells formed constitutive clusters of different sizes and densities. In the lateral part of the tectum, the maximum number of CBS$^+$ cells and their conglomerates were found in *pia mater*.

In the periventricular layer, which is a zone of primary proliferation, we also identified intensely labeled cells. This is consistent with the previously expressed assumption about the involvement of H_2S in cell proliferation processes in the tectum (Pushchina et al., 2011). Thus, the patterns of CBS immunopositivity in the intact tectum correspond to zones of constitutive neurogenesis, which is consistent with previously obtained data of CBS labeling in juvenile *O. masou*, the carp *C. carpio* (Pushchina et al., 2011; Pushchina and Varaksin, 2011), and juvenile trout (Pushchina et al., 2019).

As a result of UEI in the trout tectum, the number of CBS$^+$ cells increases dramatically, dense CBS$^+$ cell groups in different layers of the tectum appear, and CBS expression is induced in RG cells. The present results of CBS labeling with polyclonal antibodies in the tectum of adult trout confirm the data of IHC labeling using monoclonal antibodies in a younger age group of rainbow trout (Pushchina et al., 2019). This indicates that, at different periods of the constitutive ontogenesis in rainbow trout, UEI leads to the activation of expression in the aNSCs RG cells against the background of a general decrease in the number of CBS-immunopositive neuroepithelial cells detected in intact animals. The data of quantitative analysis showed that in the lateral part of the tectum, the distribution density of RG is greater than that in the dorsal and medial parts, while the average number of reactive neurogenic niches in these areas remains approximately the same. In all the tectum layers after UEI, we observed an increase in the number of CBS$^+$ cells, reaching a maximum value in SGP. In SGC and SGAP, a significant increase in the number of CBS$^+$ cells was detected as compared with the control animal.

Post-traumatic disorders of energy metabolism that occur in the rainbow trout tectum after UEI cause a number of changes resulting from the depletion of ATP. One of the

main metabolic changes is glycolysis, which serves as the main factor of reduction in ATP-generating oxidative phosphorylation (Mergenthaler et al., 2004). Loss of ATP leads to an imbalance of ionic homeostasis in tectum cells due to the breakdown of ATP-ases or ATP-dependent ion transporters (Kalogeris et al., 2012), which regulate the influx of calcium and sodium. These changes lead to an outflow of potassium due to the subsequent depletion of ATP and calcium accumulation (Katsura et al., 1994; Mark et al., 2001). An increase in intracellular calcium leads to glutamate, which increases calcium overload and activates calcium-dependent lipases and proteases (Mark et al., 2001). Such shifts in ionic homeostasis lead to an increase in the production of reactive oxygen species (ROS), the opening of transitional pores of mitochondrial permeability, inflammation, and neuron death (White et al., 2000; Kalogeris et al., 2012). In intact animals, astrocytes surrounding the neurons absorb extracellular glutamate and protect neurons from excitotoxicity (Mergenthaler et al., 2004; Wang et al., 2014). However, during brain injury, damaged astrocytes may exacerbate ischemic reperfusion injury due to inhibition of the main glutamate transporter (GLT1) (Li et al., 2011; Wang et al., 2014).

Thus, as a result of UEI, a number of pathophysiological changes develop in the trout tectum and, as a consequence, result in oxidative stress. *In vivo* experiments indicate that the role of H_2S is performed in many ways to prevent oxidative stress, including the glutathione cycle, activation of enzymes and transcription factors related to redox balance (Kimura, 2013). It is believed that one of the pathophysiological effects in rainbow trout after UEI should be the polarization of microglia with the appearance of clusters of activated microglia having a pro-inflammatory phenotype. Similar effects were also observed in a cell culture with exogenous administration of sodium hydrosulfide (Zhang et al., 2017). Thus, the increase in H_2S production in the rainbow trout brain after UEI should be considered in terms of maintaining cerebrovascular homeostasis, implying anti-apoptotic, anti-inflammatory, and antioxidant effects, and reducing the level of secondary neuronal damage resulting from oxidative stress.

Cerebellum

CBS localization was carried out in the cerebellar body and granule eminences of trout. Earlier studies on juvenile rainbow trout with monoclonal antibodies against CBS showed the presence of H_2S-producing complexes in the granular layer and *valvula cerebelli* (Pushchina et al., 2019). The data from this study showed that H_2S production varies significantly between different neuroanatomical regions of CCb, in particular, among GL cells. The highest number of CBS^+ cells was observed in the dorso-lateral and dorso-medial parts of CCb, in the basal part: the medial and lateral number of immunopositive cells was lower. A quantitative evaluation of the CBS^+ elements of the ganglionic layer of CCb was carried out for the first time. In DLP, CBS^+ Purkinje cells prevailed over CBS^- Purkinje cells; in BLP, *vice versa*. In the medial zones of the rainbow trout CCb, dorsal and basal, typical CBS^+ eurydendroid neurons were observed. The proportion of CBS-positive and negative Purkinje cells in BMP and DMP was almost the same, and the number of CBS^+ EDCs was higher in BMP than in DMP. Thus, in CCb of rainbow intact trout, we identified a heterogeneous population of Purkinje cells, some of which were CBS-positive, and the others were CBS-negative. The distribution of CBS^+ and CBS^- CPs in CCb was characterized by a certain spatial specificity: most of the CBS^+ CPs were localized in the DLP. In the basal and dorsal parts of CCb, CBS^+ EDCs, forming extracerebellar projections, were observed.

An essential feature of CBS immunopositivity of projection cells of rainbow trout GL is their relationship with CBS^+ glial-like cells. Similar patterns of colocalization of moderately labeled CPs and EDCs with small, intensely labeled cells were characteristic of all CCb areas, and were also observed in the adjacent areas of GrL and ML. In most cases, small, intensely labeled astrocyte-like cells and/or microglia attached to weakly or moderately labeled large EDCs or Purkinje cells. Such a neuro/glial-like/microglial construction corresponds to the established model of intercellular relationships, in which glial cells are the main source of H_2S for neurons (Hu et al., 2007; Lee et al., 2009). The relationship with neurons is a pre-requisite for the release of H_2S from astrocytes and the increase in intracellular calcium in astrocytes (Nagai et al., 2004). H_2S activates the transition potential of A1 channels (TRPA1) of the transition receptor, leading to an influx of calcium and activation of astrocytes by transmitting calcium waves after neuronal activation (Nagy and Winterbourn, 2010). Further, D-serine is released from astrocytes, subsequently activating NMDA receptors (Kimura, 2013). Thus, neuron/glial-like relationships were identified in CCb and granular eminences of intact trout, in which H_2S is very likely to be released from astrocyte-like cells with subsequent activation of NMDA receptors in neurons. Such features of the organization of H_2S-producing trout cell complexes are consistent with the physiological principles established in a mammalian model, according to which astrocyte-like cells in the fish cerebellum regulate the amount of glutamate produced and its reuptake, preventing the effects of excitotoxicity and providing effective conditions for neurotransmission (Kimura, 2013; Kimura et al., 2013).

Unlike monoclonal antibodies, the use of polyclonal antibodies in the cerebellum of rainbow trout makes it possible to identify the cell complexes with greater clarity. Nevertheless, the results of this work largely complement the previously obtained data on juvenile masu salmon (Pushchina et al., 2011; Pushchina and Varaksin, 2011) and rainbow trout (Pushchina et al., 2019).

Another area of CCb in intact rainbow trout containing intensely labeled CBS^+ cells is the DMZ and ML surface layers. In the GrE of rainbow trout, surface accumulations of CBS^+ cells of the neuroepithelial phenotype with a high level of enzyme activity were also detected. These areas of cerebellum are associated with the processes of constitutive proliferation and neurogenesis, which corresponds to the presence

of CBS^+ areas in the matrix zones of the rainbow trout telencephalon and tectum. The CBS expression in progenitor cells indicates the synthesis of H_2S and the subsequent increase in intracellular calcium. H_2S, similarly to nitric oxide (NO), is known to provide post-translational modifications of proteins by adding extra sulfur atom(s) to reactive cysteine residues by S-sulfhydration (Paul and Snyder, 2012). It is assumed that sulfhydration plays an important role in the activation or inactivation of many classes of proteins, including ion channels, such as ATP-dependent potassium channels, TRPV3, TRPV6, TRPM (Liu et al., 2014), enzymes and transcription factors (NF-kB, Nrf2) (Paul and Snyder, 2012). All these processes are particularly intensive in cells with an increased proliferative potential, which explains the expression of CBS in the matrix zones of the rainbow trout cerebellum. Bound sulfur, or sulfan-sulfur, is found in various proteins and is formed by adding sulfur to elemental sulfur or adding sulfur to disulfide, which can lead to the formation of polysulfides (Ogasawara et al., 1994). Bound sulfur acts as a source of sulphide accumulation and can perform regulatory control of proteins (Kimura et al., 2012). It is also efficiently released from neurons and astrocytes in the presence of glutathione (GSH), a cellular antioxidant.

In the parenchymal layers of the granular eminences of rainbow trout, CBS^+ cells were present; their spatial localization and structural organization generally corresponded to those in the granular layer of CCb. In the basal part of GrE, CBS^+ fibers ascending from the inferior olive complex of brainstem were observed. The results obtained are consistent with the previously obtained data of CBS immunolabeling of liana-like fibers in the cerebellum of masu salmon (Pushchina et al., 2011; Pushchina and Varaksin, 2011) and carp (Pushchina et al., 2011).

After UEI in the cerebellum of trout, the number of CBS^+ cells in the ML increased dramatically, indicating a sharp activation of ATP-dependent processes in this area. Along with the increase in the number of immunopositive cells, the number of CBS^+ clusters of cells increased, both in the surface and deeper parts of the ML. Numerous neurogenic niches were reactivated; patterns of neuron/glia-like/microglial colocation were observed not only in the GrL, but also in the ML. CBS^+ fibers, absent in intact animals, were observed. In neuron/glia-like complexes, glial-like cells were very intensely labeled, which indicates an increase in CBS activity. As we believe, this increase in the number of CBS^+ cells is due to the oxidative stress and the accumulation of ROS, which are neutralized by H_2S. The sources of ROS generation in cells include mitochondria, superoxide-producing enzymes such as xanthine oxide, NADPH oxidase, and H_2S-producing enzymes such as superoxide dismutase (Li et al., 2011; Jiang et al., 2013). ROS acceptors include antioxidants such as glutathione and the enzymes: superoxide disumutase and catalase. The modulation of ion channels and inflammatory and antioxidant transcription factors using H_2S after UEI may play a protective role in reducing oedema and inflammation (Kimura et al., 2006; Lee et al., 2009; Xiao et al., 2012). Similar effects have been reported for culture of endothelial cells and hippocampal neurons with the addition of donors of H_2S Na_2S (50 mM) or NaHS (50 and 250 mM), which increase the activity of antioxidant enzymes such as superoxide dismutase, catalase, and glutathione peroxidase (Hu et al., 2015; Yu et al., 2015).

In vivo experiments indicate that the role of H_2S is performed in many ways to control oxidative stress, including the glutathione cycle, enzyme activation, and transcription factors related to redox balance (Islam et al., 2015). Astrocytes provide cysteine as an important source of producing GSH in neurons (Bridges et al., 2012). In experiments on the mammalian brain, the incorporation of H_2S donors NaSH (100 mM) weakened excitotoxicity and increased intracellular GSH levels in a dose-dependent manner in a primary culture of neurons (Kimura and Kimura, 2004). Experiments with the inclusion of a metabolic radiolabel confirm the incorporation of L-cysteine, generated by trans-sulfurization of CBS and cystathionine γ-lyase (CSE), into glutathione in astrocytes and neurons (Vitvitsky et al., 2006). These studies suggest that H_2S may be useful to enhance the mechanism of cellular antioxidant protection in the brain.

Substantial structural changes occurred in the DMZ and superficial CBS^+ cell clusters were observed in rainbow trout after UEI. The number of CBS^+ cells in the surface clusters and the number of CBS^+ cells in subventricular and deeper ML sites increased. In the DMZ, the level of enzyme activity in undifferentiated cells decreased, and the number of CBS^+ cells increased. At the same time, a reactive zone containing a group of intensely labeled CBS^+ cells, which are absent in intact animals, appeared in the apical region. This redistribution of CBS immunopositivity in the DMZ is one of the significant events that occur after UEI. In the GL and GrL, the number of CBS^+ cells increased; the induction of enzyme activity arised in new types of neurons that are negative in intact animals. Thus, in the rainbow trout cerebellum, in all layers (ML, GL and GrL) of CCb, as well as in the GrE, the number of CBS^+ cells increased after UEI. We believe that the increase in the number of H_2S-producing cells is a reaction to oxidative stress, and the subsequent overproduction of H_2S results from trans-sulfuration to neutralize ROS produced in cells due to the traumatic damage. This is the protective effect of H_2S on the cells in the cerebellum after UEI. In the zones of constitutive neurogenesis, the observed rearrangement in the DMZ is associated with the appearance of an additional CBS^+ apical zone and the decrease in enzyme activity in the constitutive DMZ.

Author contributions: *EVP designed the study, prepared animal models, performed immunohistochemistry study, analyzed experimental data, and wrote the paper. AAV and DKO participated in paper writing and provided critical revision of the paper for intellectual content. IMP performed western blot analysis and ELISA analysis. All authors approved the final version of this paper.*
Conflicts of interest: *None declared.*
Financial support: *This work was supported by a grant from the President of the Russian Federation (No. MD-4318.2015.4; to EVP), a grant from the Program for Basic Research of the Far East Branch of the Russian Academy of Sciences 2015–2017 (No. 15-I-6-116, section III to EVP, AAV and DKO).*
Institutional review board statement: *All experiments were approved by the Commission on Biomedical Ethics, A.V. Zhirmunsky National Sci-*

entific Center of Marine Biology (NSCMB), Far Eastern Branch, Russian Academy of Science (FEB RAS) (approval No. 1) on July 31, 2019.

Copyright license agreement: *The Copyright License Agreement has been signed by both authors before publication.*

Data sharing statement: *Datasets analyzed during the current study are available from the corresponding author on reasonable request.*

Plagiarism check: *Checked twice by iThenticate.*

Peer review: *Externally peer reviewed.*

Open peer reviewers: *Jigar Pravinchandra Modi, Florida Atlantic University, USA; Jenny R. Lenkowski, Goucher College, USA.*

Additional files:

Additional Figure 1: *Experimental design.*

Additional Table 1: *Morphometric parameters of $GFAP^+/GFAP^-$ cells of the optic nerves of the trout Oncorhynchus mykiss at 1 week after unilateral eye injury.*

Additional Table 2: *Morphometric parameters of CBS^+ cells in the proliferative zones and deep layers of the brain of intact trout (Oncorhynchus mykiss) and 1 week after unilateral eye injury.*

Additional file 1: *Open peer review reports 1 and 2.*

References

Adolf B, Chapouton P, Lam CS, Topp S, Tannhäuser B, Strähle U, Götz M, Bally-Cuif L (2006) Conserved and acquired features of adult neurogenesis in the zebrafish telencephalon. Dev Biol 29:278-293.

Alunni A, Vaccari S, Torcia S, Meomartini ME, Nicotra A, Alfei L (2005) Characterization of glial fibrillary acidic protein and astroglial architecture in the brain of a continuously growing fish, the rainbow trout. Eur J Histochem 49:51-60.

Arochena M., Anadón R, Díaz-Regueira SM (2004) Development of vimentin and glial fibrillary acidic protein immunoreactivities in the brain of gray mullet (Chelon labrosus), an advanced teleost. J Comp Neurol 46:413-436.

Bodega G, Suárez I, Rubio M, Villalba RM, Fernández B (1993) Astroglial pattern in the spinal cord of the adult barbel (Barbus comiza). Anat Embryol (Berl) 187:385-398.

Bradford MM (1976) A rapid and sensitive method for the quantitation of microgram quantities of protein utilizing the principle of protein-dye binding. Anal Biochem 72:248-254.

Bridges RJ, Natale NR, Patel SA (2012) System X_c^- cystine/glutamate antiporter: an update on molecular pharmacology and roles within the CNS. Br J Pharmacol 165:20-34.

Cardone B, Roots BI (1990) Comparative immunohistochemical study of glial filament proteins (glial fibrillary acidic protein and vimentin) in goldfish, octopus and snail. Glia 3:180-192.

Che X, Fang Y, Si X, Wang J, Hu X, Reis C, Chen S (2018) The role of gaseous molecules in traumatic brain injury: an updated review. Front Neurosci 12:392.

Clint SC, Zupanc GK (2001) Neuronal regeneration in the cerebellum of adult teleost fish, *Apteronotus leptorhynchus*: guidance of migrating young cells by radial glia. Brain Res Dev Brain Res 130:15-23.

Cuoghi B, Mola L (2009) Macroglial cells of the teleost central nervous system: a survey of the main types. Cell Tissue Res 338:319-332.

Dávila JC, Guirado S, de la Calle A, Marín-Girón F (1987) The intraocular portion of the optic nerve in the turtle *Mauremys caspica*. J Anat 151:189-198.

Dahl D, Crosby CJ, Sethi JS, Bignami A (1985) Glial fibrillary acidic (GFA) protein in vertebrates: immunofluorescence and immunoblotting study with monoclonal and polyclonal antibodies. J Comp Neurol 239:75-88.

De Guevara R, Pairault C, Pinganaud G (1994) Expression of vimentin and GFAP and development of the retina in the trout. C R Acad Sci III 317:737-741.

Deng J, Lei C, Chen Y, Fang Z, Yang Q, Zhang, H, Cai M, Shi L, Dong H, Xiong L (2014) Neuroprotective gases – fantasy or reality for clinical use? Prog Neurobiol 115:210-245.

Druger RK, Glasgow E, Fuchs C, Levine EM, Matthews JP, Park CY, Schechter N (1994) Complex expression of keratins in goldfish optic nerve. J Comp Neurol 340:269-280.

Fu M, Zhang W, Wu L, Yang G, Li H, Wang R (2012) Hydrogen sulfide (H2S) metabolism in mitochondria and its regulatory role in energy production. Proc Natl Acad Sci U S A 109:2943-2948.

Fujita Y, Imagawa T, Uehara M (2000) Comparative study of the lamina cribrosa and the pial septa in the vertebrate optic nerve and their relationship to the myelinated axons. Tissue Cell 32:293-301.

Ganz J, Kaslin S, Hochmann D, Freudenreich M, Brand M (2010) Heterogeneity and independence of adult neural progenitors in the zebrafish telencephalon. Glia 58:1345-1363.

García DM, Koke JR (2009) Astrocytes as gate-keepers in optic nerve regeneration – a mini-review. Comp Biochem Physiol A Mol Integr Physiol 152:135-138.

Gopalakrishnan P, Shrestha B, Kaskas AM, Green J, Alexander JS, Pattillo CB (2019) Hydrogen sulfide: therapeutic or injurious in ischemic stroke? Pathophysiology 26:1-10.

Hildebrandt TM, Grieshaber MK (2008) Three enzymatic activities catalyze the oxidation of sulfide to thiosulfate in mammalian and invertebrate mitochondria. FEBS J 275:3352-3361.

Hu R, Cai WQ, Wu XG, Yang Z (2007) Astrocyte-derived estrogen enhances synapse formation and synaptic transmission between cultured neonatal rat cortical neurons. Neuroscience 144:1229-1240.

Hu Y, Li R, Yang H, Luo H, Chen Z (2015) Sirtuin 6 is essential for sodium sulfide-mediated cytoprotective effect in ischemia/reperfusion-stimulated brain endothelial cells. J Stroke Cerebrovasc Dis 24:601-609.

Islam KN, Polhemus DJ, Donnarumma E, Brewster LP, Lefer DJ (2015) Hydrogen sulfide levels and nuclear factor-erythroid2-related factor 2 (NRF2) activity are attenuated in the setting of critical limb ischemia (CLI). J Am Heart Assoc 4:pii: e001986.

Ito Y, Tanaka H, Okamoto H, Ohshima T (2010) Characterization of neural stem cells and their progeny in the adult zebrafish optic tectum. Dev Biol 342:26-38.

Jiang X, Huang Y, Lin W, Gao D, Fei Z (2013) Protective effects of hydrogen sulfide in a rat model of traumatic brain injury via activation of mitochondrial adenosine triphosphate-sensitive potassium channels and reduction of oxidative stress. J Surg Res 184:e27-35.

Kálmán M, Ari C (2002) Distribution of GFAP immunoreactive structures in the rhombencephalon of the sterlet (Acipenser ruthenus) and its evolutionary implication. J Exp Zool 293:395-406.

Kálmán M, Gould RM (2001) GFAP-immunopositive structures in spiny dogfish, Squalus acanthias, and little skate, Raia erinacea, brains: differences have evolutionary implications. Anat Embryol (Berl) 204:59-80.

Kálmán M (1998) Astroglial architecture of the carp (Cyprinus carpio) brain as revealed by immunohistochemical staining against glial fibrillary acidic protein (GFAP). Anat Embryol (Berl) 198:409-433.

Kalogeris T, Baines CP, Krenz M, Korthuis RJ (2012) Cell biology of ischemia/reperfusion injury. Int Rev Cell Mol Biol 298:229-317.

Katsura K, Kristián T, Siesjö BK (1994) Energy metabolism, ion homeostasis, and cell damage in the brain. Biochem Soc Trans 22:991-996.

Kimura H, Shibuya N. Kimura Y (2012) Hydrogen sulfide is a signaling molecule and a cytoprotectant. Antioxid Redox Signal 17:45-57.

Kimura H (2013) Physiological role of hydrogen sulfide and polysulfide in the central nervous system. Neurochem Int 63:492-497.

Kimura Y, Dargusch R, Schubert D, Kimura H (2006) Hydrogen sulfide protects HT22 neuronal cells from oxidative stress. Antioxid Redox Signal 8:661-670.

Kimura Y, Mikami Y, Osumi K, Tsugane M, Oka J, Kimura H (2013) Polysulfides are possible H2S-derived signaling molecules in rat brain. FASEB J 27:2451-2457.

Kimura Y, Kimura H (2004) Hydrogen sulfide protects neurons from oxidative stress. FASEB J 18:1165-1167.

Lee M, Schwab C, Yu S, McGeer E, McGeer PL (2009) Astrocytes produce the anti-inflammatory and neuroprotective agent hydrogen sulfide. Neurobiol Aging 30:1523-1534.

Li L, Rose P, Moore PK (2011) Hydrogen sulfide and cell signaling Annu Rev Pharmacol Toxicol 5:169-187.

Lillo C, Velasco A, Jimeno D, Cid E, Lara J.M, Aijón J (2002) The glial design of a teleost optic nerve head supporting continuous growth. J Histochem Cytochem 50:1289-1302.

Liu H, Wang Y, Xiao Y, Hua Z, Cheng J, Jia J (2016) Hydrogen sulfide attenuates tissue plasminogen activator-induced cerebral hemorrhage following experimental stroke. Transl Stroke Res 7:209-219.

Liu Y, Yang R, Liu X, Zhou Y, Qu C, Kikuiri T, Wang S, Zandi E, Du J, Ambudkar IS, Shi S (2014) Hydrogen sulfide maintains mesenchymal stem cell function and bone homeostasis via regulation of Ca2+ channel sulfhydration. Cell Stem Cell 15:66-78.

Luo Y, Yang X, Zhao S, Wei C, Yin Y, Liu T, Jiang S, Xie J, Wan X, Mao M, Wu J (2013) Hydrogen sulfide prevents OGD/R-induced apoptosis via improving mitochondrial dysfunction and suppressing an ROS-mediated caspase-3 pathway in cortical neurons. Neurochem Int 63:826-831.

Maggs A, Scholes J (1990) Reticular astrocytes in the fish optic nerve: macroglia with epithelial characteristics form an axially repeated lacework pattern, to which nodes of Ranvier are apposed. J Neurosci 10:1600-1614.

Marcus RC, Easter SS (1995) Expression of glial fibrillary acidic protein and its relation to tract formation in embryonic zebrafish (Danio rerio). J Comp Neurol 359:365-381.

Margotta V, Morelli A (1997) Contribution of radial glial cells to neurogenesis and plasticity of central nervous system in adult vertebrates. Animal Biol 6:101-108.

Mark LP, Prost RW, Ulmer JL, Smith MM, Daniels DL, Strottmann JM, Brown WD, Hacein-Bey L (2001) Pictorial review of glutamate excitotoxicity: fundamental concepts for neuroimaging. AJNR Am J Neuroradiol 22:1813-1824.

März M, Chapouton N, Diotel C, Vaillant B, Hesl M, Takamiya CS, Lam O, Kah L, Bally-Cuif U (2010) Heterogeneity in progenitor cell subtypes in the ventricular zone of the zebrafish adult telencephalon. Glia 58:870-888.

Menuet A, Pellegrini E, Brion F, Gueguen MM, Anglade I, Pakdel F, Kah O (2005) Expression and estrogen-dependent regulation of the zebrafish brain aromatase gene. J Comp Neurol 485:304-320.

Mergenthaler P, Dirnagl U, Meisel A (2004) Pathophysiology of stroke: lessons from animal models. Metab Brain Dis 19:151-167.

Nagai Y, Tsugane M, Oka J, Kimura H (2004) Hydrogen sulfide induces calcium waves in astrocytes. FASEB J 18:557-559.

Nagy P, Winterbourn C (2010) Rapid reaction of hydrogen sulfide with the neutrophil oxidant hypochlorous acid to generate polysulfides. Chem Res Toxicol 23:1541-1543.

Northcutt RG (2008) Forebrain evolution in bony fishes. Brain Res Bull 75:191-205.

Ogasawara Y, Isoda S, Tanabe S (1994) Tissue and subcellular distribution of bound and acid-labile sulfur, and the enzymic capacity for sulfide production in the rat. Biol Pharm Bull 17:1535-1542.

Olson KR, Donald JA, Dombkowski RA Perry SF (2012) Evolutionary and comparative aspects of nitric oxide, carbon monoxide and hydrogen sulfide. Respir Physiol Neurobiol 184:117-129.

Onteniente B, Kimura H, Maeda T (1983) Comparative study of the glial fibrillary acidic protein in vertebrates by PAP immunohistochemistry. J Comp Neurol 141:283-312.

Parrilla M, Lillo C, Herrero-Turrión MJ, Arévalo R, Aijón J, Lara JM, Velasco A (2013) Pax2+ astrocytes in the fish optic nerve head after optic nerve crush. Brain Res 1492:18-32.

Parrilla M, Lillo C, Herrero-Turrión MJ, Arévalo R, Aijón J, Lara JM, Velasco A (2012) Characterization of Pax2 expression in the goldfish optic nerve head during retina regeneration. PLoS One 7:e32348.

Parrilla M, Lillo C, Herrero-Turrion MJ, Arévalo R, Lara JM, Aijón J, Velasco A (2009) Pax2 in the optic nerve of the goldfish, a model of continuous growth. Brain Res 1255:75-88.

Paul BD, Snyder SH (2012) H2S signaling through protein sulfhydration and beyond. Nat Rev Mol Cell Biol 13:499-507.

Pushchina EV, Varaksin AA (2019) Neurolin expression in the optic nerve and immunoreactivity of Pax6-positive niches in the brain of rainbow trout (Oncorhynchus mykiss) after unilateral eye injury. Neural Regen Res 14:156-171.

Pushchina EV, Shukla S, Varaksin AA, Obukhov DK (2016b) Cell proliferation and apoptosis in optic nerve and brain integration centers of adult trout Oncorhynchus mykiss after optic nerve injury. Neural Regen Res 11:578-590.

Pushchina EV, Varaksin AA, Obukhov DK (2019) Cystathionine β-synthase in the brain of the trout Oncorhynchus mykiss after unilateral eye damage and in conditions of in vitro cultivation. Russ J Dev Biol 50:39-58.

Pushchina EV, Varaksin AA, Obukhov DK (2011) Cystathionine β-synthase in the CNS of masu salmon Oncorhynchus masou (Salmonidae) and carp Cyprinus carpio (Cyprinidae). Neurochem J 5:24-34.

Pushchina EV, Varaksin AA, Obukhov DK (2016a) Reparative neurogenesis in the brain and changes in the optic nerve of adult trout Oncorhynchus mykiss after mechanical damage of the eye. Russ J Dev Biol 47:11-32.

Pushchina EV, Varaksin AA, Obukhov DK (2018) The Pax2 and Pax6 transcription factors in the optic nerve and brain of trout Oncorhynchus mykiss after a mechanical eye injury. Russ J Dev Biol 49:264-290.

Pushchina EV, Varaksin AA (2011) Hydrogen sulfide, parvalbumin-, and GABA-producing system in the masu salmon brain. Neurophysiology 43:109-122.

Somogyi P, Eshhar N, Teichberg VI, Roberts JD (1990) Subcellular localization of a putative kainate receptor in Bergmann glial cell using a monoclonal antibody in the chick and fish cerebellar cortex. Neuroscience 35:9-30.

Than-Trong E, Bally-Cuif L (2015) Radial glia and neural progenitors in the adult zebrafish central nervous system. Glia 63:1406-1428.

Tomizawa K, Inoue Y, Nakayasu HA (2000) Monoclonal antibody stains radial glia in the adult zebrafish (Danio rerio) CNS. J Neurocytol 29:119-128.

Vitvitsky V, Thomas M, Ghorpade A, Gendelman HE, Banerjee R (2006) A functional transsulfuration pathway in the brain links to glutathione homeostasis. J Biol Chem 281:35785-35793.

Wang JF, Li Y, Song JN, Pang HG (2014) Role of hydrogen sulfide in secondary neuronal injury. Neurochem Int 64:37-47.

Wang R (2012) Physiological implication of hydrogen sulfide: a which exploration that blossomed. Physiol Rev 92:791-896.

Wasowicz M, Ward R, Reperant J (1999) An investigation of astroglial morphology in Torpedo and Scyliorhinus. J Neurocytol 28:639-653.

White BC, Sullivan JM, DeGracia DJ, O'Neil BJ, Neumar RW, Grossman LI, Rafols JA, Krause GS (2000) Brain ischemia and reperfusion: molecular mechanisms of neuronal injury. J Neurol Sci 179(S 1-2):1-33.

Whitfield NL, Kreimier EL, Verdial FC, Skovgaard N, Olson KR (2008) Reappraisal of H2S/sulfide concentration in vertebrate blood and its potential significance in ischemic preconditioning and vascular signaling. Am J Physiol Regul Integr Comp Physiol 294:R1930-1937.

Xiao L, Lan A, Mo L, Xu W, Jiang N, Hu F, Feng J, Zhang C (2012) Hydrogen sulfide protects PC12 cells against reactive oxygen species and extracellular signal-regulated kinase 1/2-mediated downregulation of glutamate transporter-1 expression induced by chemical hypoxia. Int J Mol Med 30:1126-1132.

Yoshida M (2001) Intermediate filament proteins define different glial subpopulations. J Neurosci Res 3:284-289.

Yu Q, Lu Z, Tao L, Yang L, Guo Y, Yang Y, Sun X, Ding Q (2015) ROS-dependent neuroprotective effects of NaHS in ischemia brain injury involves the PARP/AIF pathway. Cell Physiol Biochem 36:1539-1551.

Zhang M, Wu X, Xu Y, He M, Yang J, Li J, Li Y, Ao G, Cheng J, Jia J (2017) The cystathionine β-synthase/hydrogen sulfide pathway contributes to microglia-mediated neuroinflammation following cerebral ischemia. Brain Behav Immun 66:332-346.

Zupanc GK, Sîrbulescu RF (2011) Adult neurogenesis and neuronal regeneration in the central nervous system of teleost fish. Eur J Neurosci 34:917-929.

C-Editor: Zhao M; S-Editor: Li CH; L-Editor: Song LP; T-Editor: Jia Y

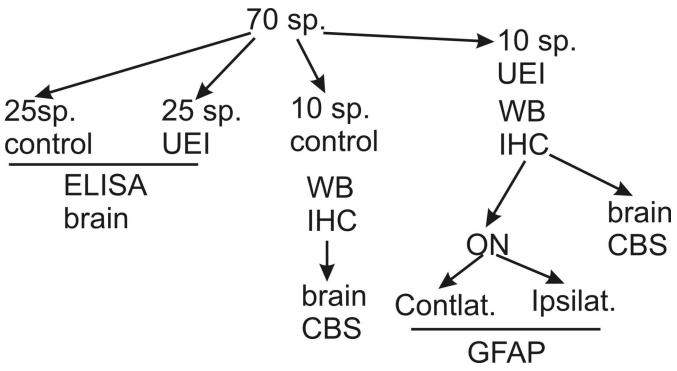

Additional Figure 1 Experimental design.

CBS: Cystathionine β-synthase; Contlat.: contralateral nerve; ELISA: enzyme-linked immunosorbent assay; GFAP: glial fibrillary acidic protein; IHC: immunohistochemistry; Ispsilat.: ipsilateral nerve; ON: optic nerve; sp: *Oncorhynchus mykiss*; UEI: unilateral eye injury; WB: western blot analysis.

Additional Table 1 Morphometric parameters of GFAP$^+$/GFAP$^-$ cells of the optic nerves of the trout *Oncorhynchus mykiss* at 1 week after unilateral eye injury

Cell type	Small cell size (μm)	Intermediate cell size (μm)	Elongated cell size (μm)	Large cell size (μm)	Nuclei size (μm)
GFAP$^+$ ipsilateral, fibrous	6.1±0.6/3.2±0.9	7.9±0.6/3.3±1.0	9.7±0.5/3.2±0.7	12.6±0.9/3.9±0.7	3.8±0.7/2.5±0.5
GFAP$^+$ ipsilateral, activated	5.4±0.5/1.7±0.2	8.1±0.5/1.8±0.4	9.9±0.5/1.8±0.4	14.1±2.0/2.0±0.4	–
GFAP$^-$ ipsilateral	–	7.7±0.5/2.7±0.7	10.2±0.7/2.9±0.7	–	5.6±0.8/2.9±0.4
GFAP$^+$ contralateral, fibrous	5.7±0.6/2.9±0.6	7.9±0.5/3.6±0.9	9.7±0.5/3.8±0.5	–	3.9±0.6/2.5±0.6
GFAP$^+$ contralateral, activated	5.9±0.6/1.9±0.2	8.2±0.6/1.8±0.3	10.2±0.6/2.2±0.3	12±0.6/2.6±0.7	–
GFAP$^-$ contralateral	5.7±0.7/3.1±0.7	8.1±0.6/2.9±0.5	10.4±0.9/2.8±0.2	–	4.2±0.5/2.8±0.4

Data are shown as the mean ± SD. GFAP: Glial fibrillary acidic protein.

Additional Table 2 Morphometric parameters of CBS$^+$ cells in the proliferative zones and deep layers of the brain of intact trout (*Oncorhynchus mykiss*) and 1 week after unilateral eye injury

Brain areas Cell type	Intact animals		Damaged optic nerve		
	Cell size (μm)	Optical density (UOD)	Cell type	Cell size (μm)	Optical density (UOD)
Telencephalon					
Dm		–	Undifferentiated	7.7±0.2/4.8±0.4	+++
Undifferentiated	–				
Oval	9.0±0.5/8.0±0.6	+++	Oval	8.7±0.5/5.7±0.6	+++
	11.1±0.6/7.8±1.2	++		11.0±0.5/6.1±0.7	++
Dd					
Undifferentiated	4.6±0.9/3.2±0.7	+++	Oval	7.7±0.2/4.8±0.4	+++/++
Oval	9.0±0.4/7.5±2.4	+++	Oval	8.7±0.5/5.7±0.6	+++
		++		10.9±0.5/6.1±0.8	++
Dl					
Undifferentiated	6.6±1.2/5.6±1.9		Undifferentiated	7.7±0.6/5.3±0.8	+++
Oval	8.8±0.6/6.2±1.4	+++	Oval	8.8±0.5/5.9±0.8	+++
	11.9±1.8/7.1±1.3	++		10.7±0.5/6.1±0.7	++
Dc			Undifferentiated	3.9±0.5/2.8±0.4	+++
Undifferentiated	5.4±0.9/3.8±0.8	+++		6.0±0.6/4.2±0.6	+++
Oval	7.7±0.5/5.0±1.3	+++	Oval	7.4±0.2/4.7±0.6	+++
	9.8±0.2/5.7±1.0	++		9.5±0.6/4.9±0.6	++
Vl	5.8±0.3/3.6±0.6	+++	Undifferentiated	6.3±0.5/4.3±0.5	+++
Undifferentiated					
Oval	9.0±0.8/6.0±1.0	+++	Oval	7.5±0.2/5.0±0.5	+++
	12.2±1.4/7.6±1.2	++		9.4±0.8/5.3±1.4	++
Vm		+++	Undifferentiated	5.6±0.3/4.5±0.6	++
Undifferentiated	5.2±1.2/3.9±0.9			6.4±0.2/5.0±0.6	++
oval	8.8±0.8/4.9±0.8	+++	Oval	7.7±0.6/5.5±0.9	++
		++		10.2±1.4/5.7±1.3	+++
Vd	–	–	Undifferentiated	5.4±0.3/4.0±0.4	+++
				6.5±0.4/4.5±0.6	+++
	–	–	Oval	7.3±0.2/4.1±0.8	++
Vv	–	–	Undifferentiated	5.5±0.3/4.3±0.6	+++
				6.6±0.3/4.9±0.7	+++
–	–	–	Oval	7.7±0.6/5.0±1.2	+++
				10.4±0.8/5.3±0.8	+++
Tectum					
SM					
Undifferentiated	4.4±0.1/3.1±0.2	+++	Undifferentiated	5.3±0.3/3.5±0.3	+++/++
				4.5±0.4/3.0±0.5	+++
Oval	7.9±1.3/4.2±0.6	+++	Oval	8.8±0.9/4.7±0.2	+++
				7.3±0.2/4.0±0.4	+++
				6.5±0.3/4.0±0.8	+++
	–	–	Radial glia	8.1±0.9/3.6±0.6	+++
				6.4±0.5/3.4±0.6	+++
SGAP					
Undifferentiated	5.2±0.4/4.3±0.5	++	Undifferentiated	5.6±0.3/4.4±0.6	+++
				6.5±0.3/5.0±0.4	+++
	–	–	Oval	10.4±0.3/5.0±1.0	+++
				8.7±0.6/5.4±1.3	+++
				7.5±0.3/5.1±0.6	+++
			Bipolar	11.7±0.4/5.5±0.4	+++
Pia mater					
Undifferentiated	5.6±0.7/4.3±1.1	+++	Undifferentiated	6.9±0.3/4.8±0.5	+++
Oval	7.9±0.8/4.5±0.5	+++	–	–	
SGP					
Undifferentiated	4.1±0.3/3.1±0.2	+++	Undifferentiated	6.1±0.4/4.5±0.6	
Oval	5.4±0.9/3.2±0.5	+++	Oval	8.2±0.5/5.2±0.7	

Additional Table 2 Continued

Brain areas Cell type	Intact animals		Damaged optic nerve		
	Cell size (μm)	Optical density (UOD)	Cell type	Cell size (μm)	Optical density (UOD)
SGC					
	–	–	Oval	10.6±0.5/7.0±0.5	+++
				9.2±0.3/8.1±0.2	+++
	–		Bipolar	11.3±0.5/5.1±0.3	+++
Undifferentiated	6.1±0.3/4.1±0.6	++	Undifferentiated	6.5±0.5/3.6±0.4	+++
Cerebellum					
CCb					
BMP					
PC	26.6±1.4/15.9±3.7	++	PC	26.5±3.7/14.5±1.7	++
	17.7±4.6/11.4±0.1	+++		15.9±2.3/11.8±2.4	++/+++
EDC	20.3±6.0/7.9±0.1	+++	EDC	33.0±2.8/11.5±1.0	+++/++
Glial-like cells	7.3±1.5/5.9±1.6	+++	Glial-like cells	7.5±1.0/4.4±1.2	++/+++
				9.7±0.4/6.5±0.9	+++
GrL					
Elongated	24.5±5.1/10.1±3.2	++	Elongated	23.0±2.5/13.3±1.8	+++/++
	14.5±0.2/9.7±0.1	++		15.0±1.3/9.4±0.5	+++/++
Oval	10.6±1.5/8.9±1.0	+++	Undifferentiated*	6.6±0.4/4.2±0.3	+++
ML					
Oval	10.1±0.7/6.7±1.3	+++	Elongated*	11.4±1.6/4.7±1.3	+++
			Oval	8.0±0.6/5.3±1.7	+++/++
			Undifferentiated*	6.3±0.6/4.6±0.8	+++/++
BLP					
PC	22.5±0.8/16.9±0.7	+++/++	PC	24.0±0.7/13.9±2.8	+++/++
	15.2±3.1/10.3±3.8	+++/++		15.3±1.7/8.8±1.4	+++
EDC	–	–	EDC	39.1±1.6/13.9±2.3	+++
				25.7±3.1/13.9±2.9	+++/++
Glial-like cells	8.2±0.3/6.2±1.0	+++	Glial-like cells	6.7±1.4/5.4±0.6	+++
ML					
Superficial cells	4.8±0.7/2.9±0.3	+++	Migrated	6.9±1.2/4.1±1.3	–
Undifferentiated	5.2±0.7/3.7±0.7	+++	Undifferentiated	5.3±0.6/3.4±0.5	+++
GrL					
Oval	11.6±3.2/7.3±1.4	++/+++			
Undifferentiated	5.2±0.9/3.5±0.9	+++	Undifferentiated	5.1±0.3/5.1±0.7	+++
DLP					
PC	25.0±4.5/15.9±3.6	++	PC	14.9±2.7/8.0±0.6	++
	15.4±1.1/12.3±1.4	++/+++	PC+ glial-like cells	7.9±0.6/4.7±0.8	+++
				5.7±0.7/5.4±0.5	+++
GrL					
Multipolar	28.0±4.5/13.7±2.4	+	Multipolar	25.0±2.4/13.6±1.8	+++/++
Heterogenous	18.4±1.2/10.5±2.9	++/+++	Oval	16.0±1.2/9.4±0.7	+++/++
Oval	11.7±3.0/9.4±3.2	+++	Undifferentiated*	6.4±0.6/4.3±0.4	+++
ML					
Oval	8.1±1.3/4.7±0.9	+++	Oval	8.5±0.5/4.9±0.6	+++
Undifferentiated	5.5±0.3/3.7±0.9	+++	Superficial cells	6.8±0.1/5.4±0.2	+++
				5.6±0.7/3.5±0.7	+++
DMP					
PC	29.2±4.0/15.5±2.8	++/+++	PC	24.3±3.6/15.6±0.9	++
	20.3±2.3/12.7±2.6	++		17.6±2.2/11.6±2.9	++
DMZ					
Undifferentiated	5.4±1.2/3.9±1.0	+++	Undifferentiated	5.3±1.0/2.7±0.5	+++
GrL					
Elongated	18.7±1.8/9.3±0.7	++/+++	Elongated	26.5±2.8/14.1±1.8	++
Oval	12.7±2.1/8.8±1.8	++/+++	Oval	13.5±1.8/9.3±1.7	++

Additional Table 2 Continued

Brain areas	Intact animals		Damaged optic nerve		
Cell type	Cell size (μm)	Optical density (UOD)	Cell type	Cell size (μm)	Optical density (UOD)
ML					
Undifferentiated	5.7±0.9/3.3±0.6	+++	Oval	7.5±0.5/4.5±1.2	+++
Superficial cells	5.3±1.1/3.3±0.4	+++	Undifferentiated	5.7±0.6/3.3±0.9	+++
			Superficial cells	4.7±0.3/3.3±0.5	+++
GrL, Caudal part of CCb					
Heterogenous			Homogeneous		
Large	26.0±4.9/13.4±1.6	++	Large	34.0±2.1/6.5±0.7	++
Medial-size	16.1±1.9/11.4±1.3	++		27.5±3.5/13.9±1.8	++
Homogenous			Medial-sized	14.5±2.1/9.4±1.7	++
Oval	11.9±4.1/7.5±3.7	+++	Oval	9.3±0.2/7.3±1.0	+++
Undifferentiated	5.2±0.4/3.8±0.2	+++	Undifferentiated	5.3±0.4/3.9±0.5	+++
Granular eminentia					
Multipolar:					
Type 1	22.0±1.6/11.5±2.0	+++	Multipolar	17.8±1.3/14.8±1.4	++
Type 2	23.3±1.6/13.6±2.3	++	Bipolar	24.6±1.3/7.11±1.2	++
Type 3	15.8±3.6/11.6±3.1	+++/++	Oval	8.9±1.1/6.7±1.1	+++
Oval	8.3±0.8/5.7±1.0	+++	Undifferentiated	6.5±1.0/4.0±0.5	+++/++
Superficial cells	5.4±0.9/4.1±0.7	+++	Superficial cells	5.4±1.2/4.3±0.3	+++

Data are shown as the mean ± SD. Optical density (OD) in CBS^+ cells was categorized by the following scale: high (160–120 UOD, corresponding to +++), moderate (120–80 UOD, corresponding to ++), weak (80–40 UOD, corresponding to +), and low (less than 40 UOD, corresponding to –); the initial OD value was measured on the control mounts. Large and small diameters of the cell body are shown through a slash. Cells were morphologically classified according to a previously developed scheme (Pushchina et al., 2018). *indicates additional cell types that appear in the cerebellum after injury. BLP: Baso-lateral part of cerebellar body; BMP: baso-medial part of cerebellar body; CCb: cerebellar body; Dc: dorso-central region of telencephalon; Dd: dorso-dorsal region of telencephalon; Dl: dorso-lateral region of telencephalon; DLP: dorso-lateral part of cerebellar body; Dm: dorso-medial region of telencephalon; DMP: dorso-medial part of cerebellar body; EDC: euryndroid cells; GrL: granular layer; ML: molecular layer; PC: Purkinje cells; SM: *stratum marginale*; SGAP: *stratum griseum et album periventriculare*; SGC: *stratum griseum centrale*; SGP: *stratum griseum periventriculare*; UOD: Unites of optical density; Vd: ventro-dorsal region of telencephalon; Vl: ventro-lateral region of telencephalon; Vm: ventro-medial region of telencephalon; Vv: ventro-ventral region of telencephalon.